This project was funded through the Illinois Department of Natural Resources and the Illinois State Geological Survey. Illinois State Water Survey Contract Report 2004-12. This document contains the report figures only.

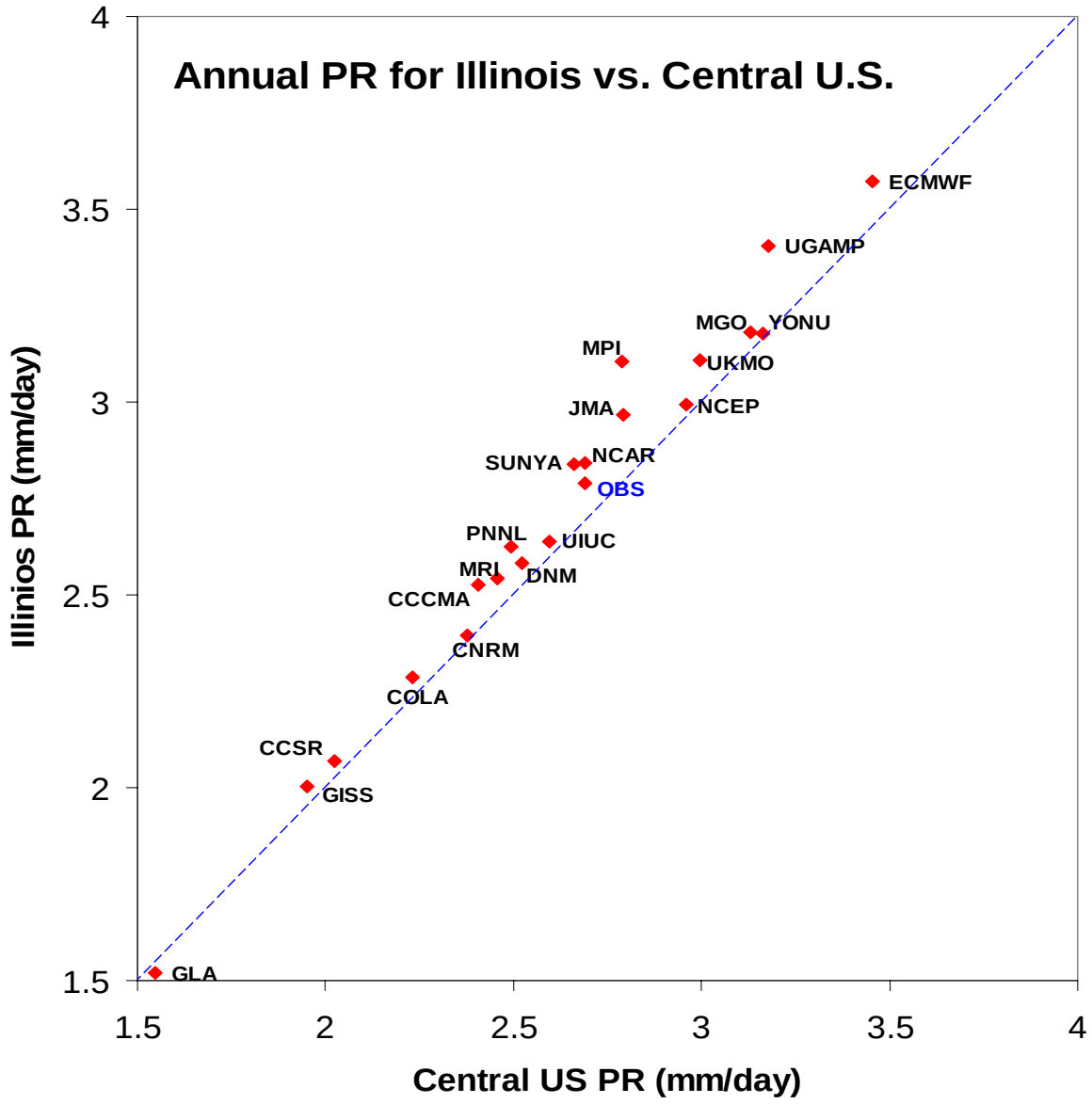

Figure 1. Annual precipitation for Illinois versus annual precipitation for central U.S. Units: mm d^{-1}. Each point represents a different AMIP model.

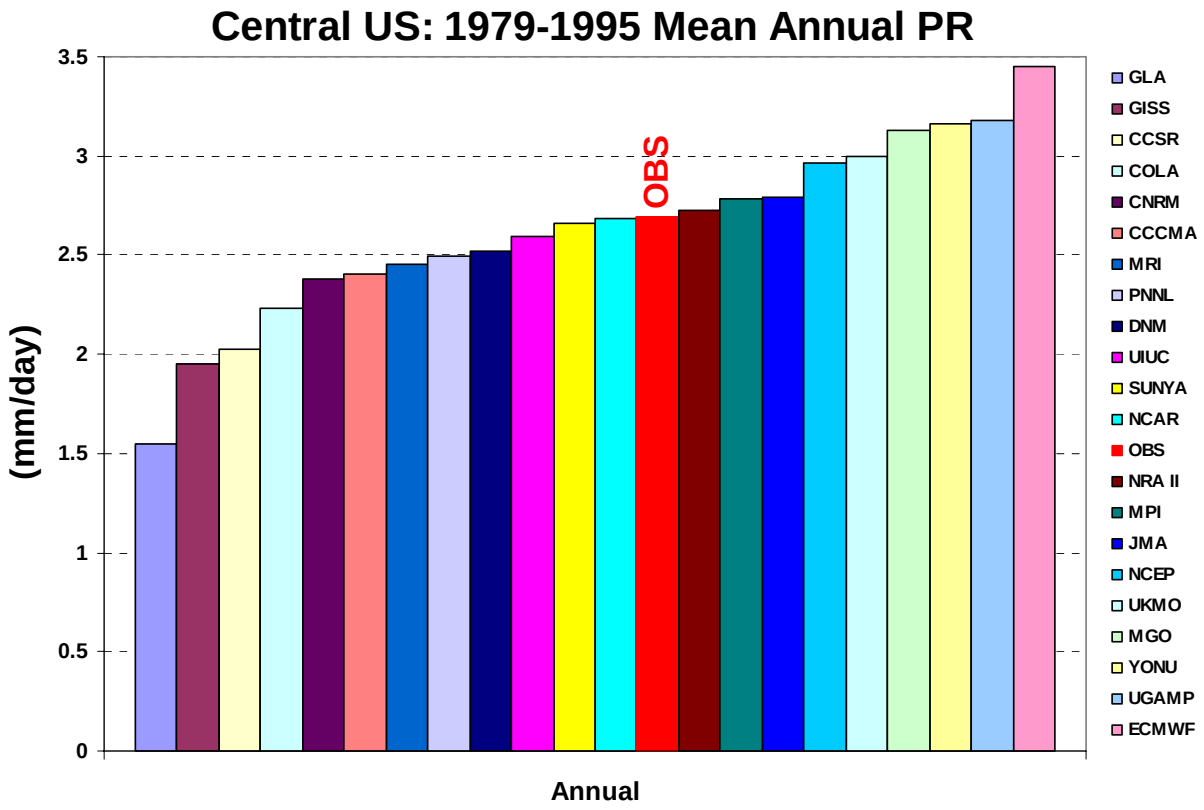

Figure 2. Annual mean precipitation (mm d^{-1}) for the central U.S. for AMIP models and observations ("OBS"). Values are plotted in order of increasing precipitation. The period covered is 1979-1995.

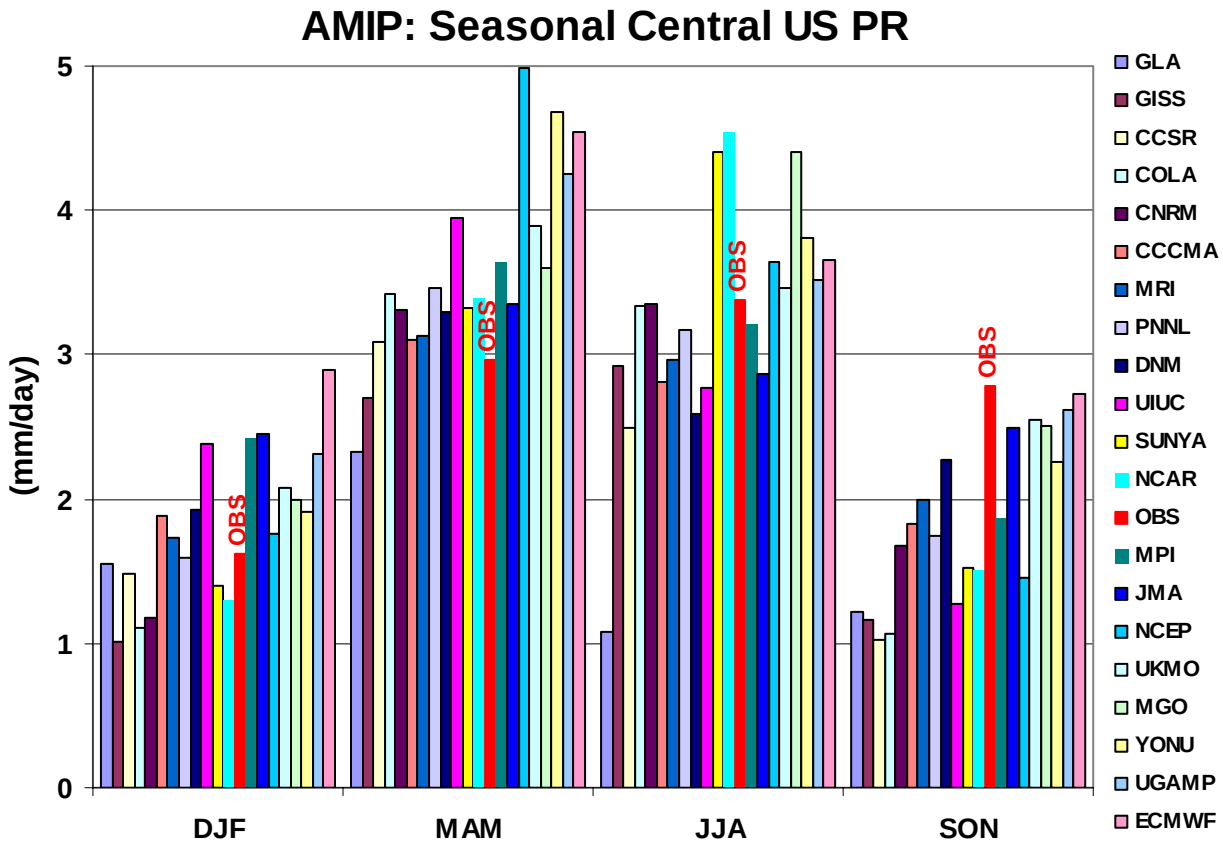

Figure 3. Seasonal (winter, spring, summer, fall) mean central U.S. precipitation (mm d^{-1}) for AMIP models and observations for the period 1979-1995.

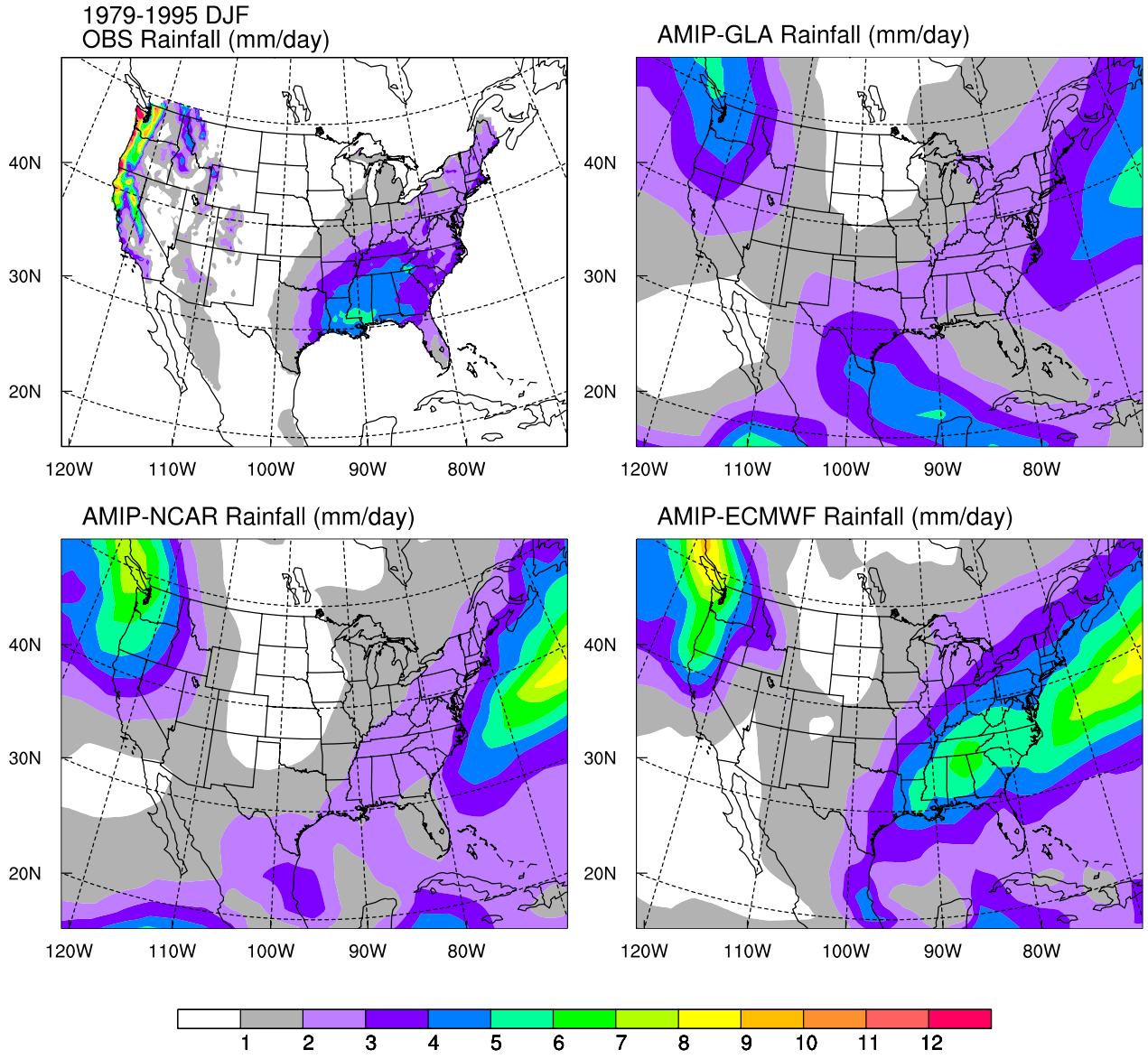

Figure 4. Maps of winter precipitation (mm d^{-1}) from observations (top left), the GLA (driest annual) model (top right), the NCAR (an intermediate) model (bottom left), and the ECMWF (wettest annual) model (bottom right).

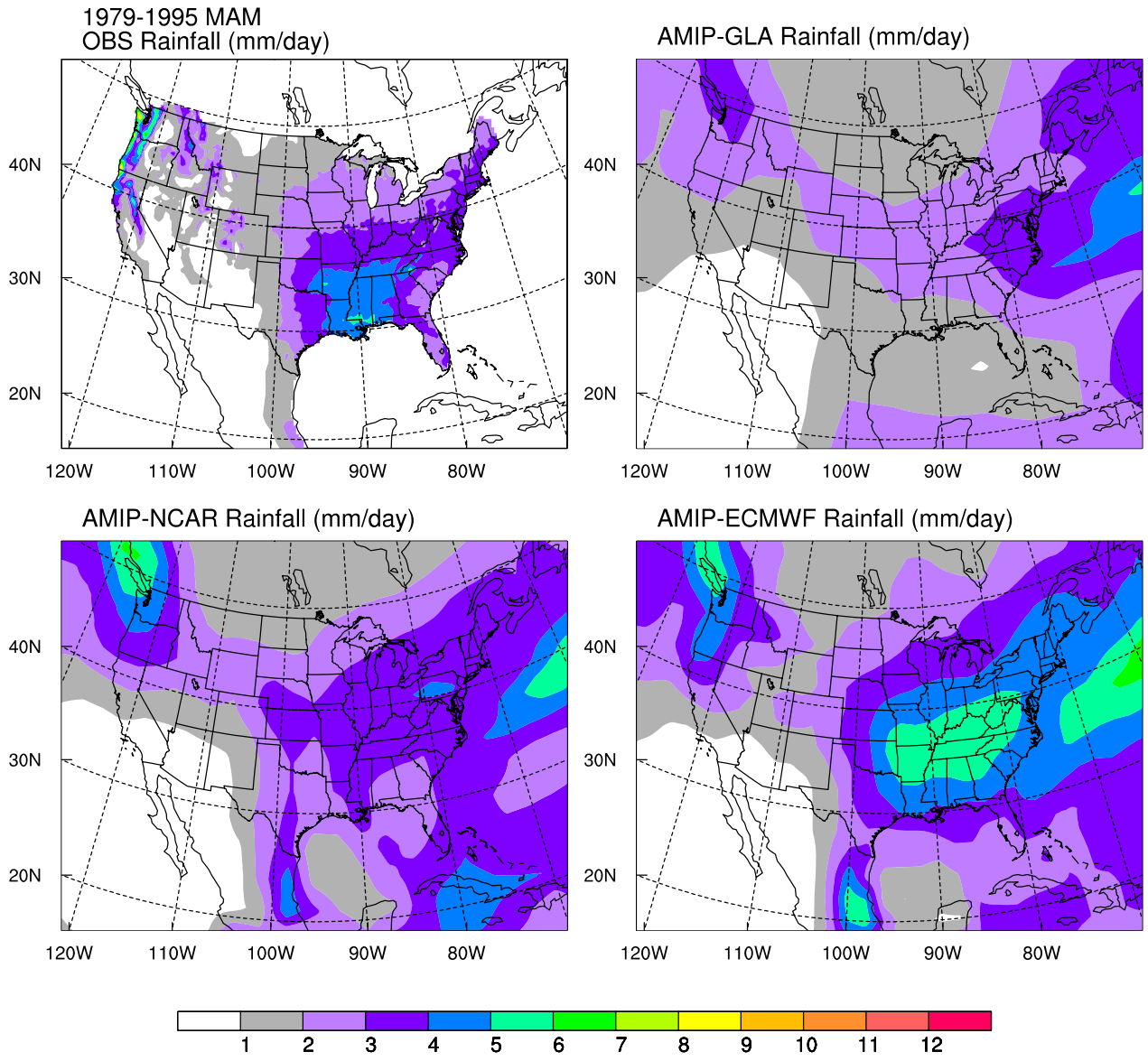

Figure 5. Maps of spring precipitation (mm d^{-1}) from observations (top left), the GLA (driest annual) model (top right), the NCAR (an intermediate) model (bottom left), and the ECMWF (wettest annual) model (bottom right).

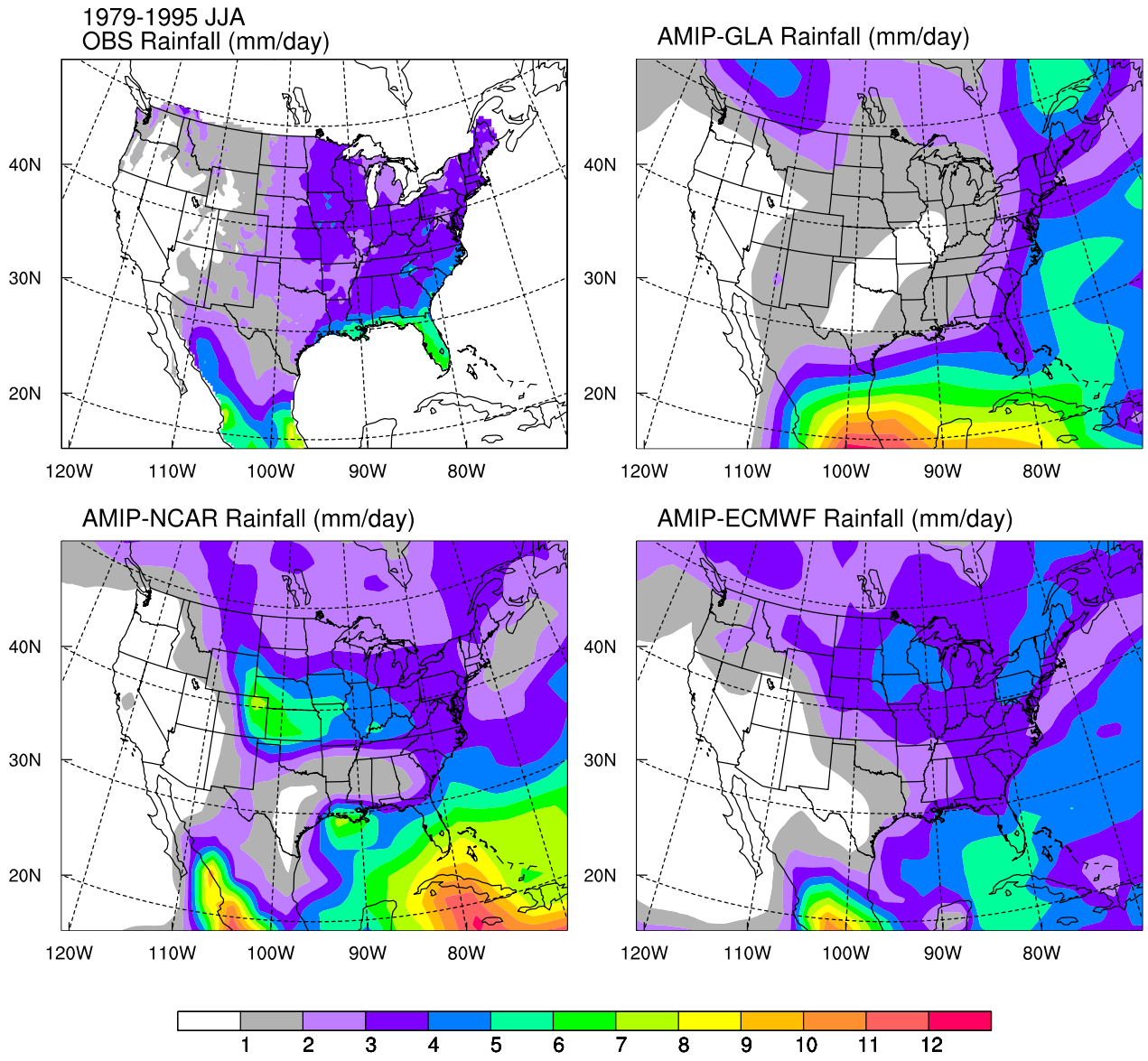

Figure 6. Maps of summer precipitation (mm d^{-1}) from observations (top left), the GLA (driest annual) model (top right), the NCAR (an intermediate) model (bottom left), and the ECMWF (wettest annual) model (bottom right).

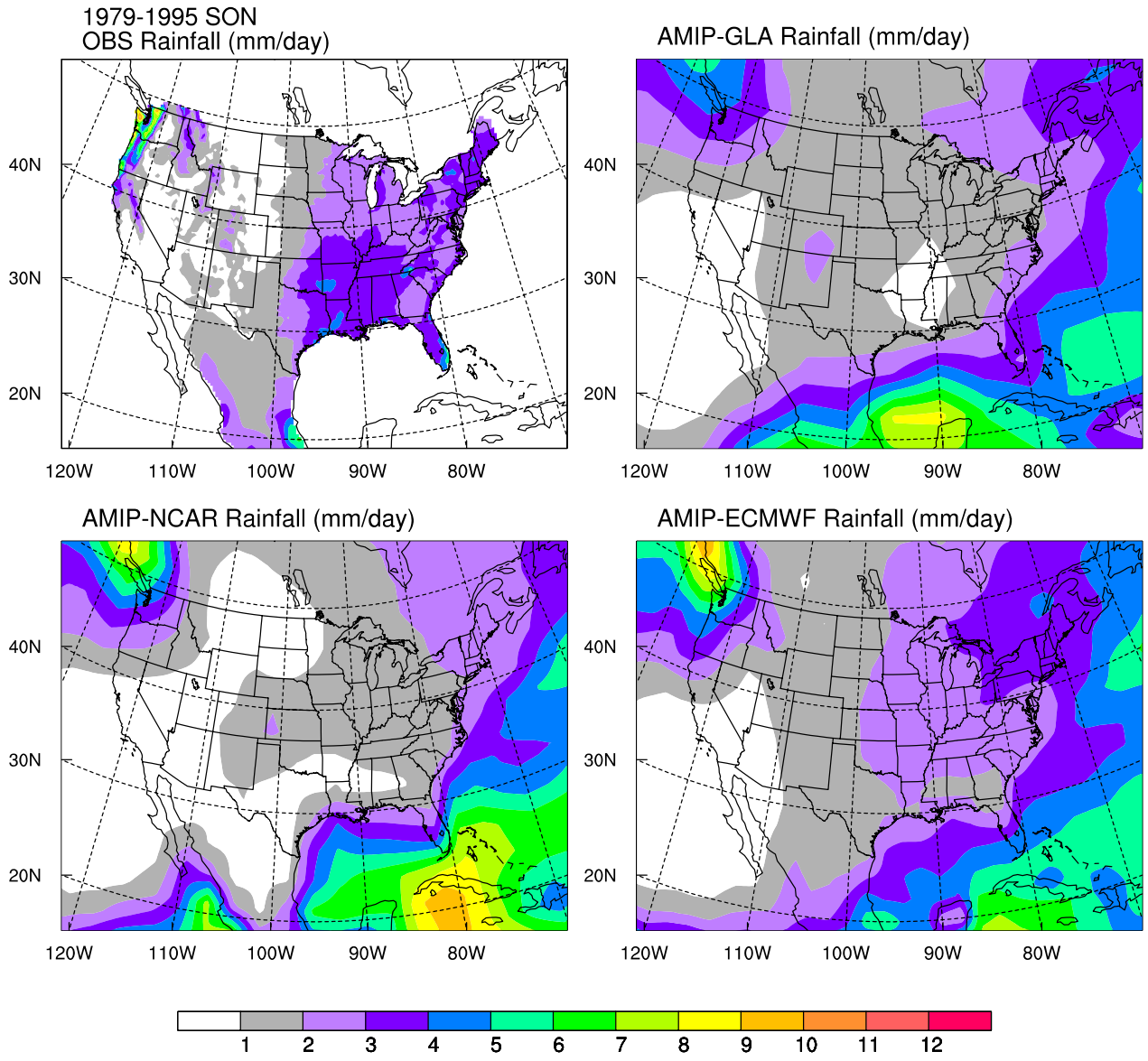

Figure 7. Maps of fall precipitation (mm d^{-1}) from observations (top left), the GLA (driest annual) model (top right), the NCAR (an intermediate) model (bottom left), and the ECMWF (wettest annual) model (bottom right).

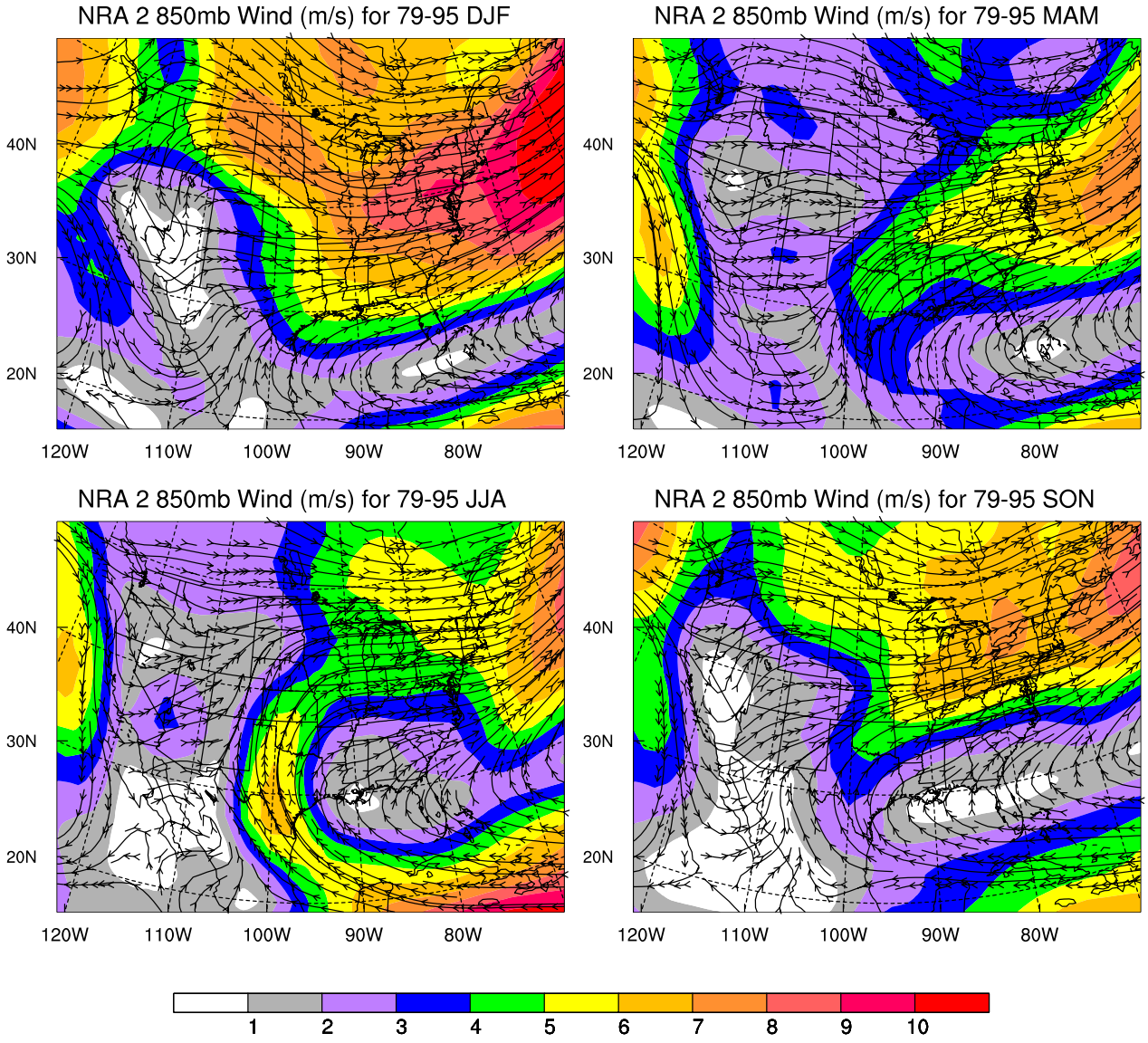

Figure 8. Map of observed (1979-1995) wind flow at a level of 850 hPa for winter (top left), spring (top right), summer (bottom left), and fall (bottom right). Barbed lines indicated wind flow directions and colored shading indicates speed (m s^{-1}).

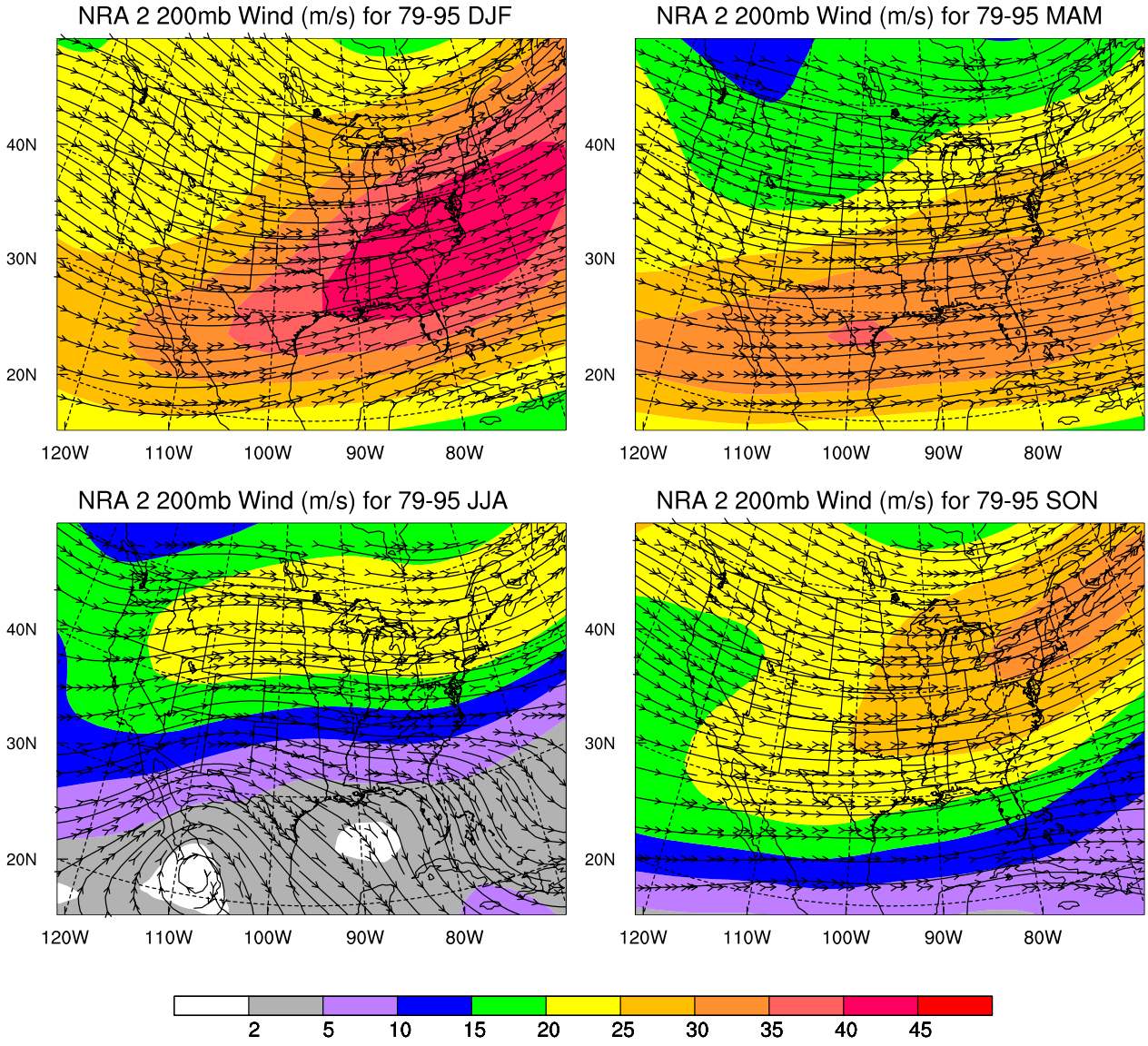

Figure 9. Map of observed (1979-1995) wind flow at a level of 200 hPa for winter (top left), spring (top right), summer (bottom left), and fall (bottom right). Barbed lines indicated wind flow directions and colored shading indicates speed (m s^{-1}).

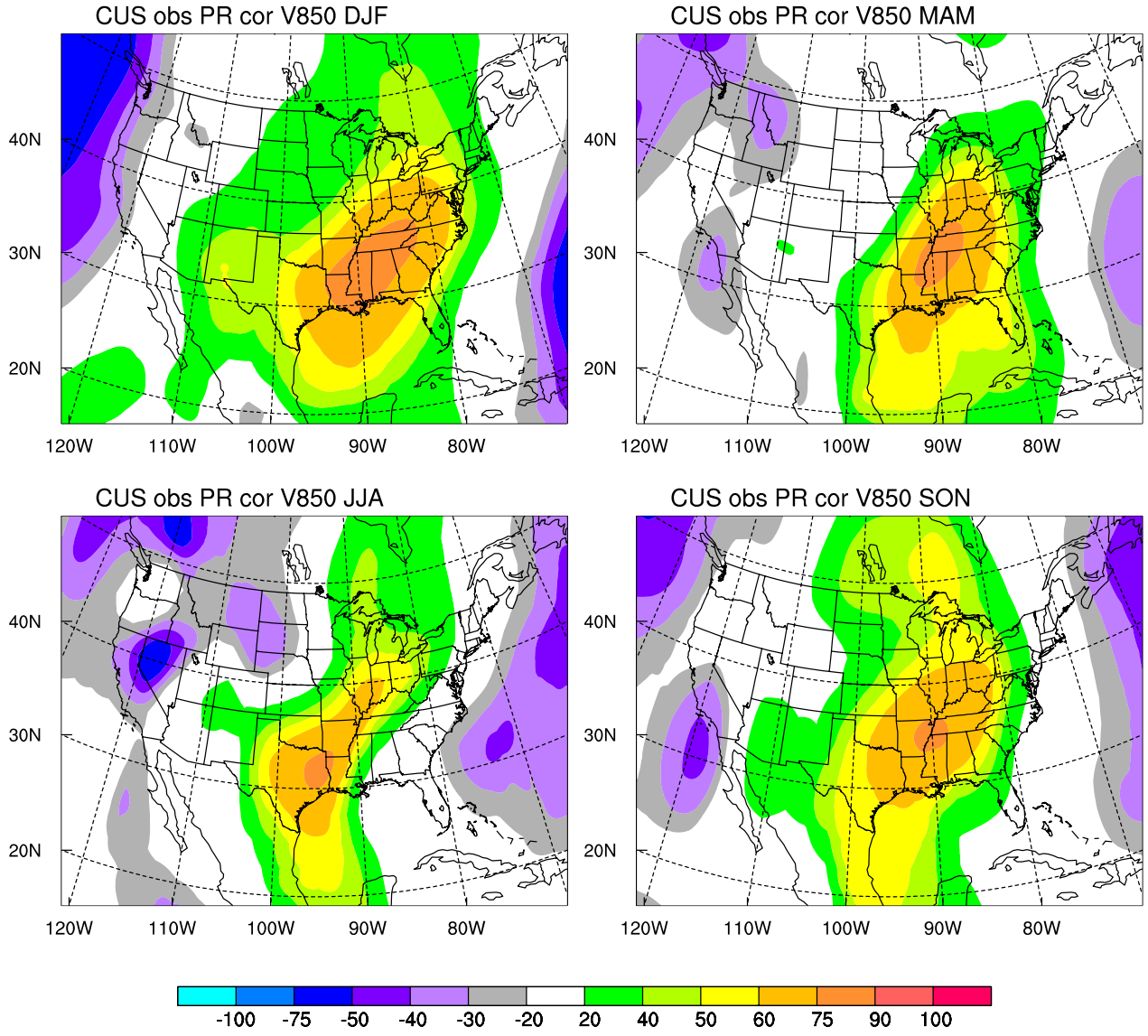

Figure 10. Maps of correlation coefficient for 1979-1995 between observed southerly component of the wind speed at 850 hPa and observed precipitation in the central U.S. for winter (top left), spring (top right), summer (bottom left), and fall (bottom right).

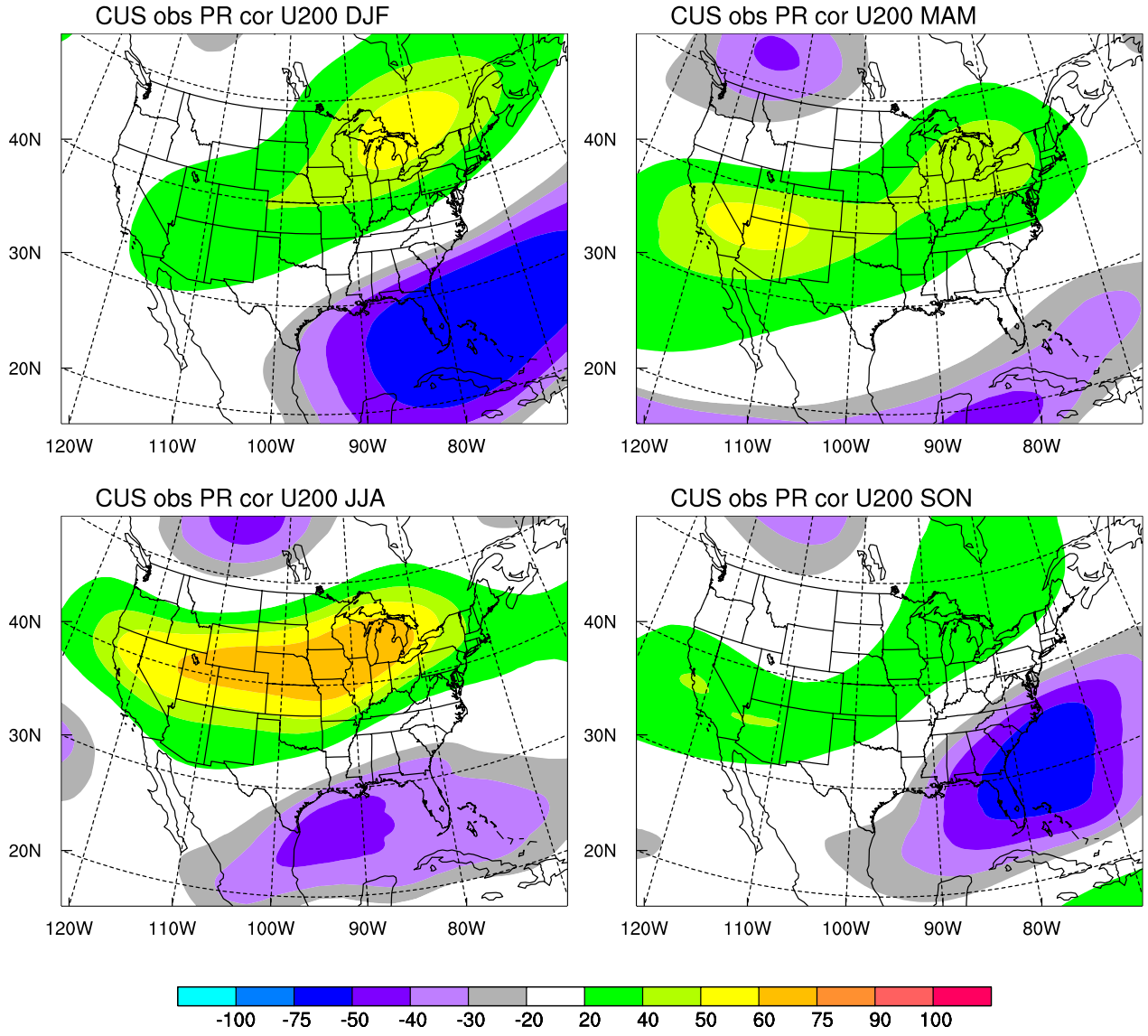

Figure 11 Maps of correlation coefficient for 1979-1995 between observed westerly component of the wind speed at 200 hPa and observed precipitation in the central U.S. for winter (top left), spring (top right), summer (bottom left), and fall (bottom right).

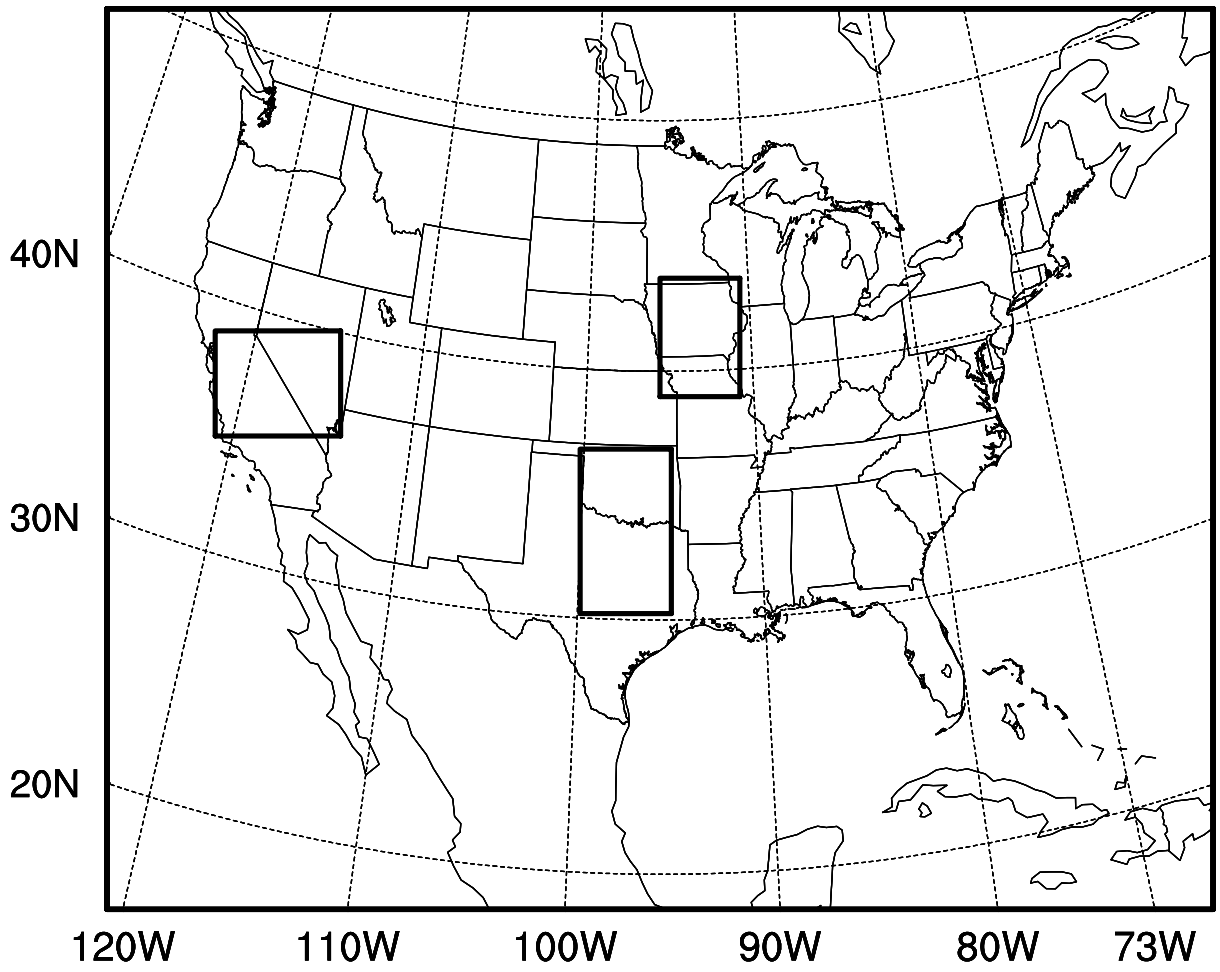

Figure 12. Locations of boxes used for analysis of GCM performance.

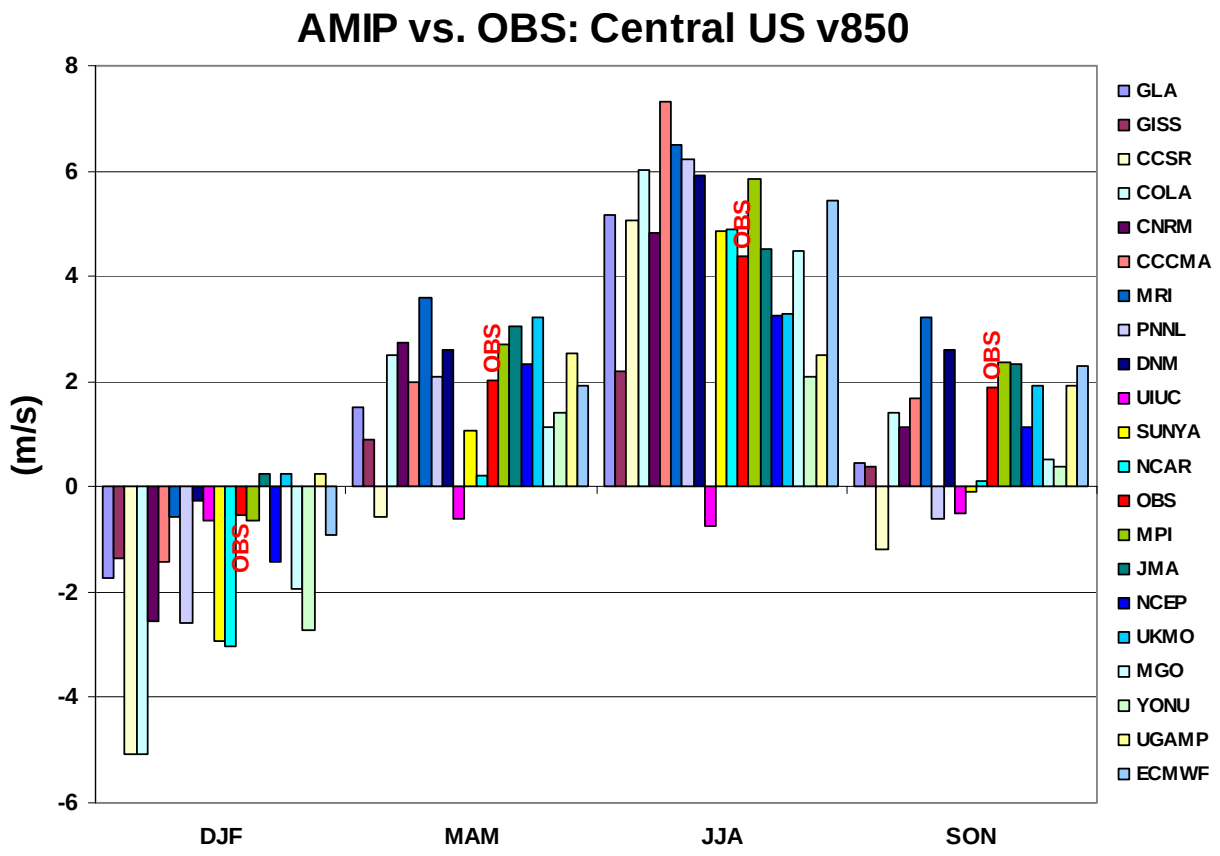

Figure 13. Southerly wind component (m s^{-1}) at 850 hPa in the LLJ region for the 4 seasons for AMIP models and observations for the period 1979-1995.

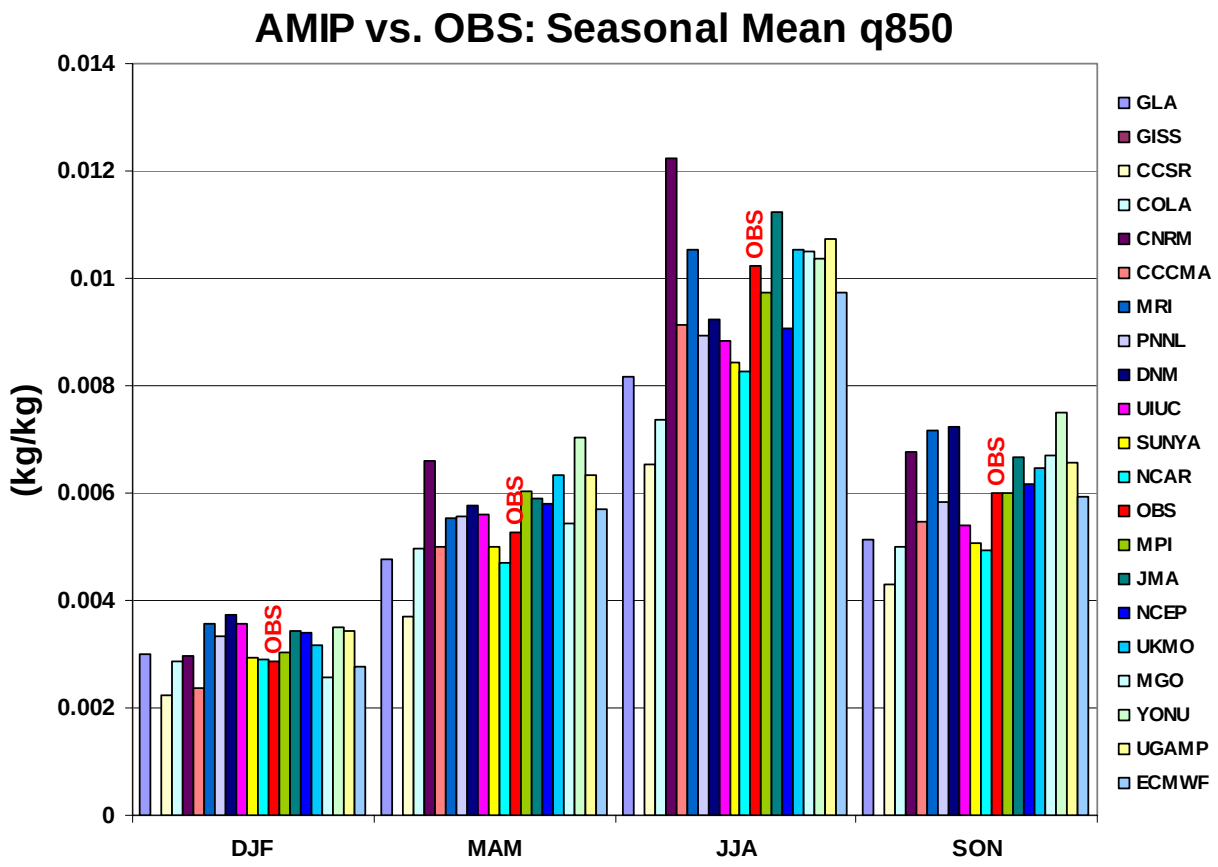

Figure 14. Specific humidity (kg H_2O/kg air) at 850 hPa in the LLJ region for the 4 seasons for AMIP models and observations for the period 1979-1995.

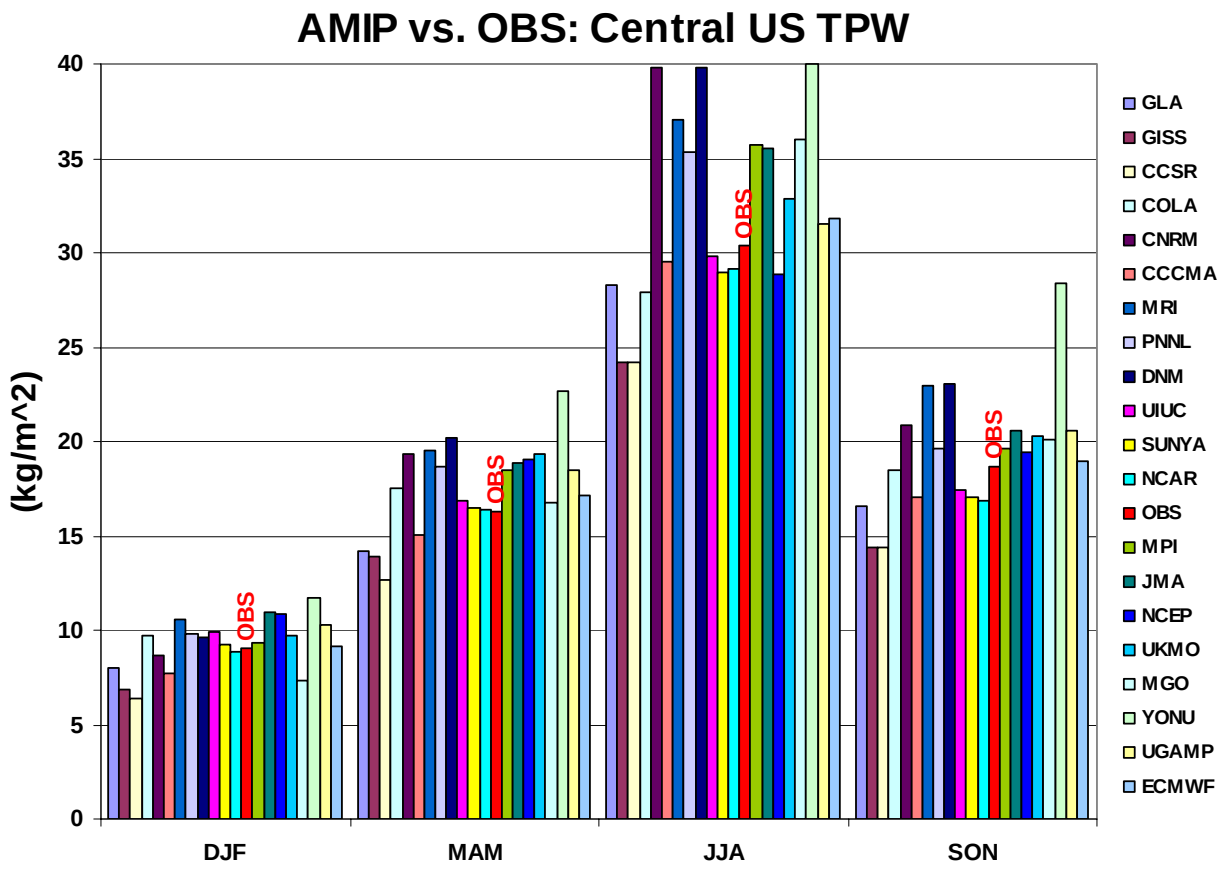

Figure 15. Total precipitable water (kg m^{-2}) over central U.S. for the 4 seasons for AMIP models and observations for the period 1979-1995.

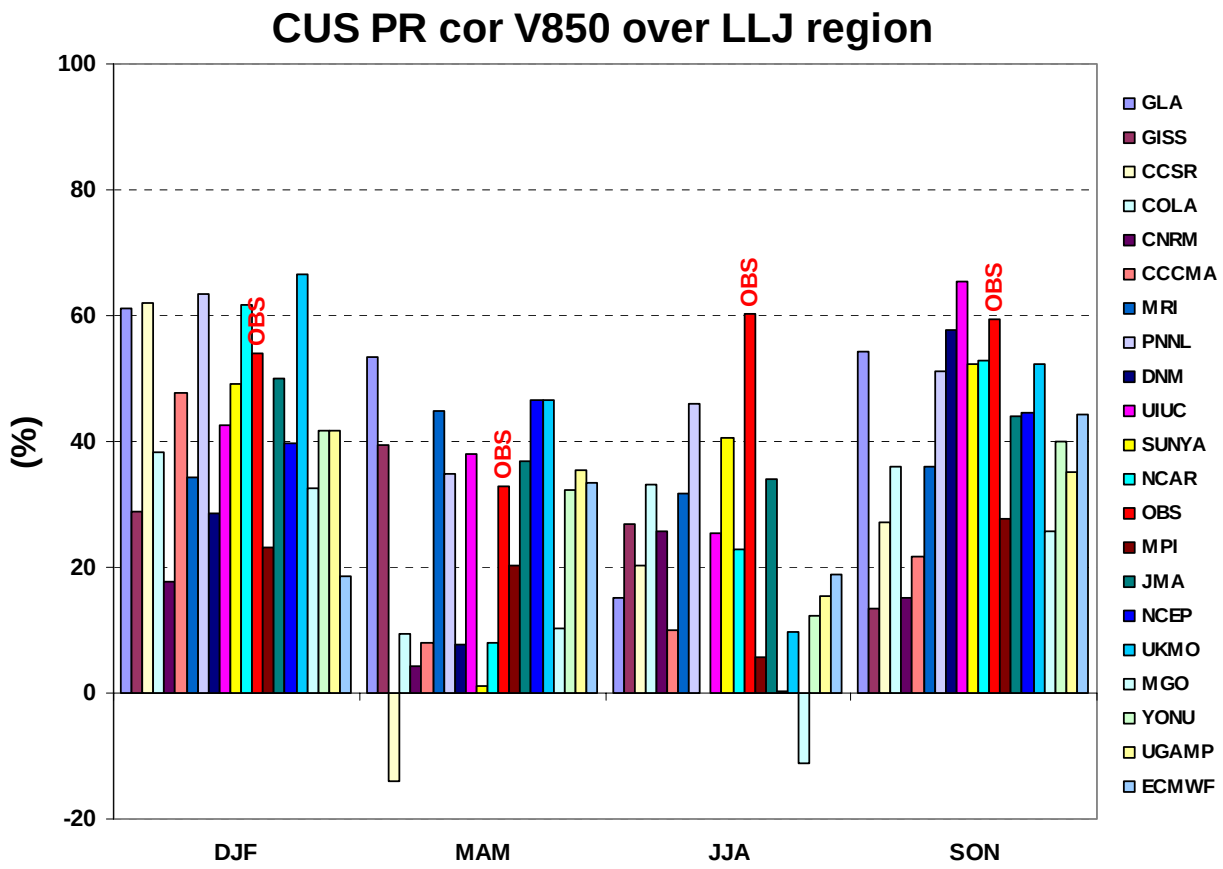

Fig.16. Correlation coefficient for 4 seasons for AMIP models between model precipitation in the central U.S. and model southerly component of the wind speed at 850 hPa in the LLJ region (Fig. 13).

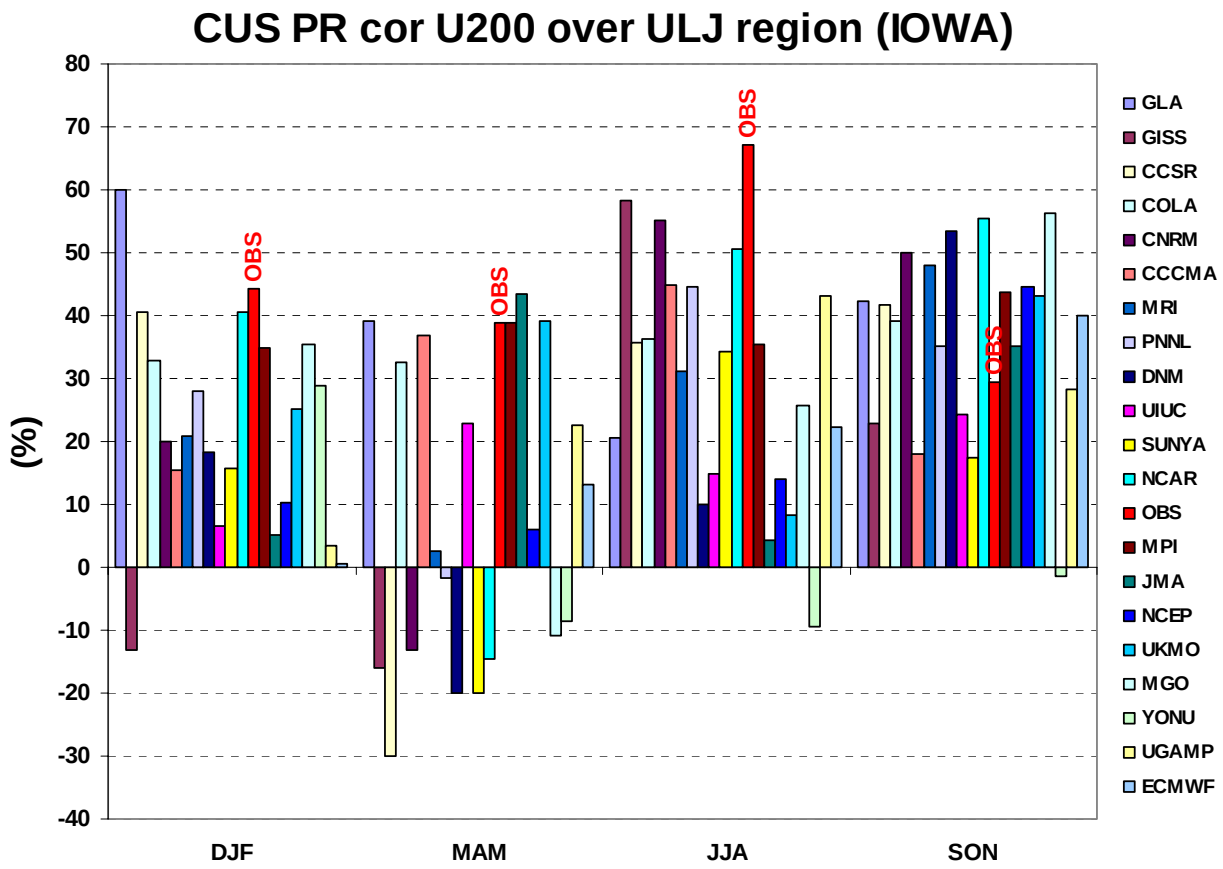

Fig. 17. . Correlation coefficient for 4 seasons for AMIP models between model precipitation in the central U.S. and model westerly component of the wind speed at 200 hPa in the Iowa region (Fig. 13)

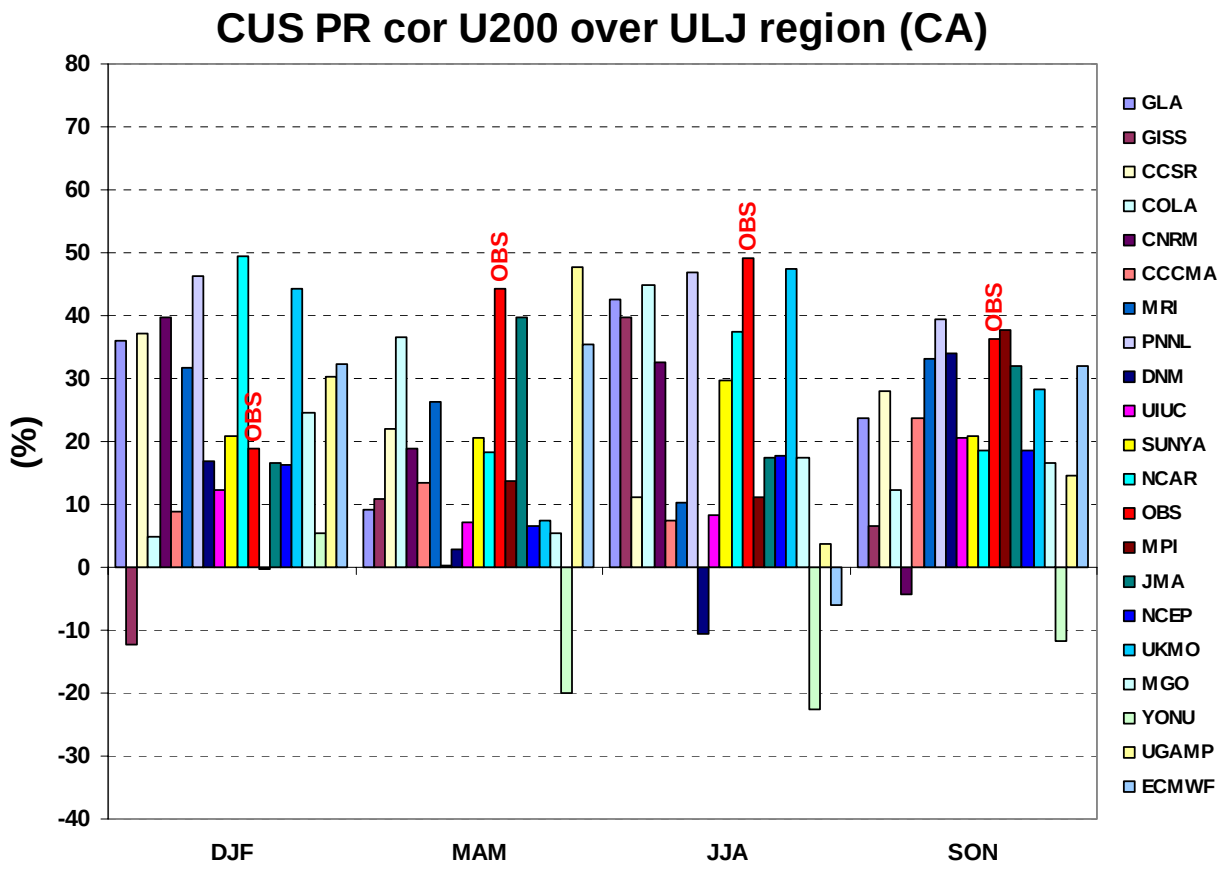

Figure 18. Correlation coefficient for 4 seasons for AMIP models between model precipitation in the central U.S. and model westerly component of the wind speed at 200 hPa in the California region (Fig. 13).

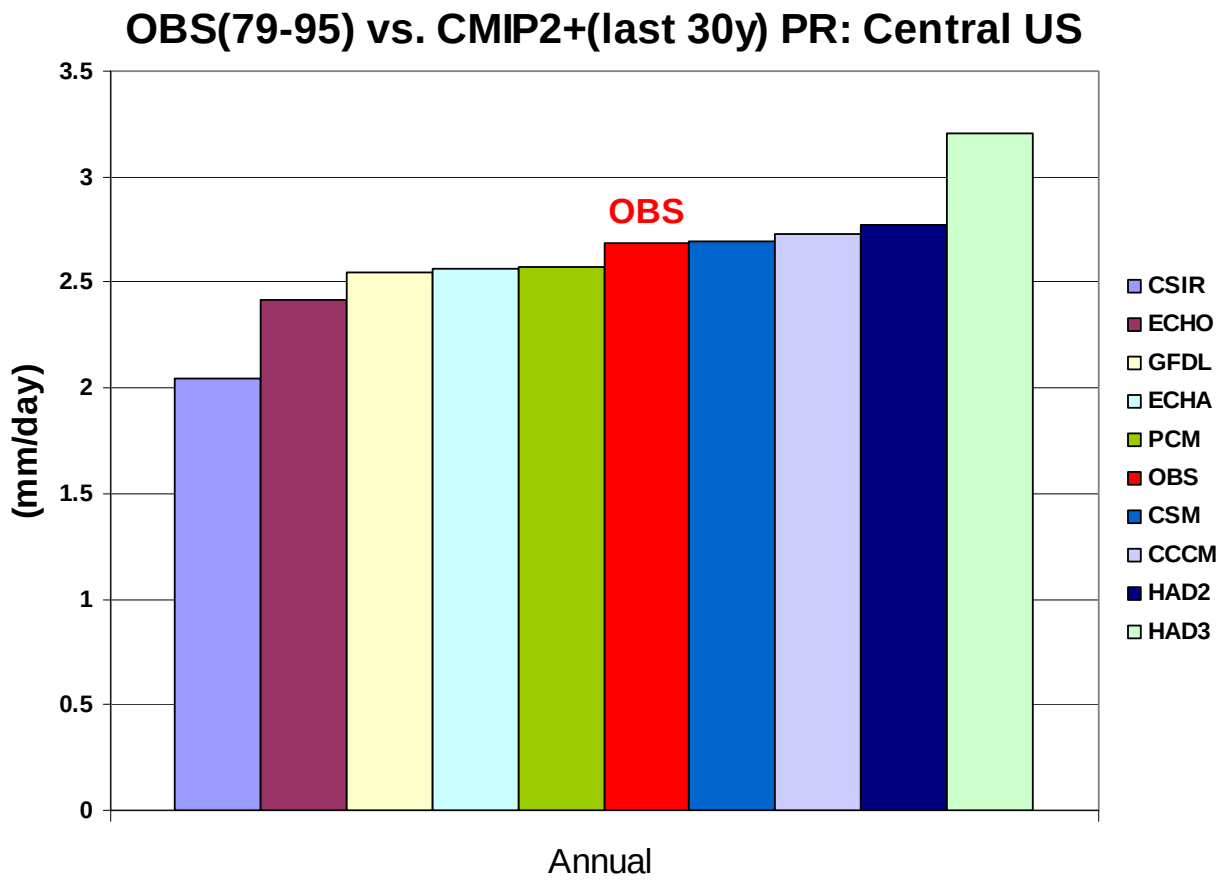

Fig. 19. Annual precipitation for the observations (1979-1995) and the control runs of CMIP models.

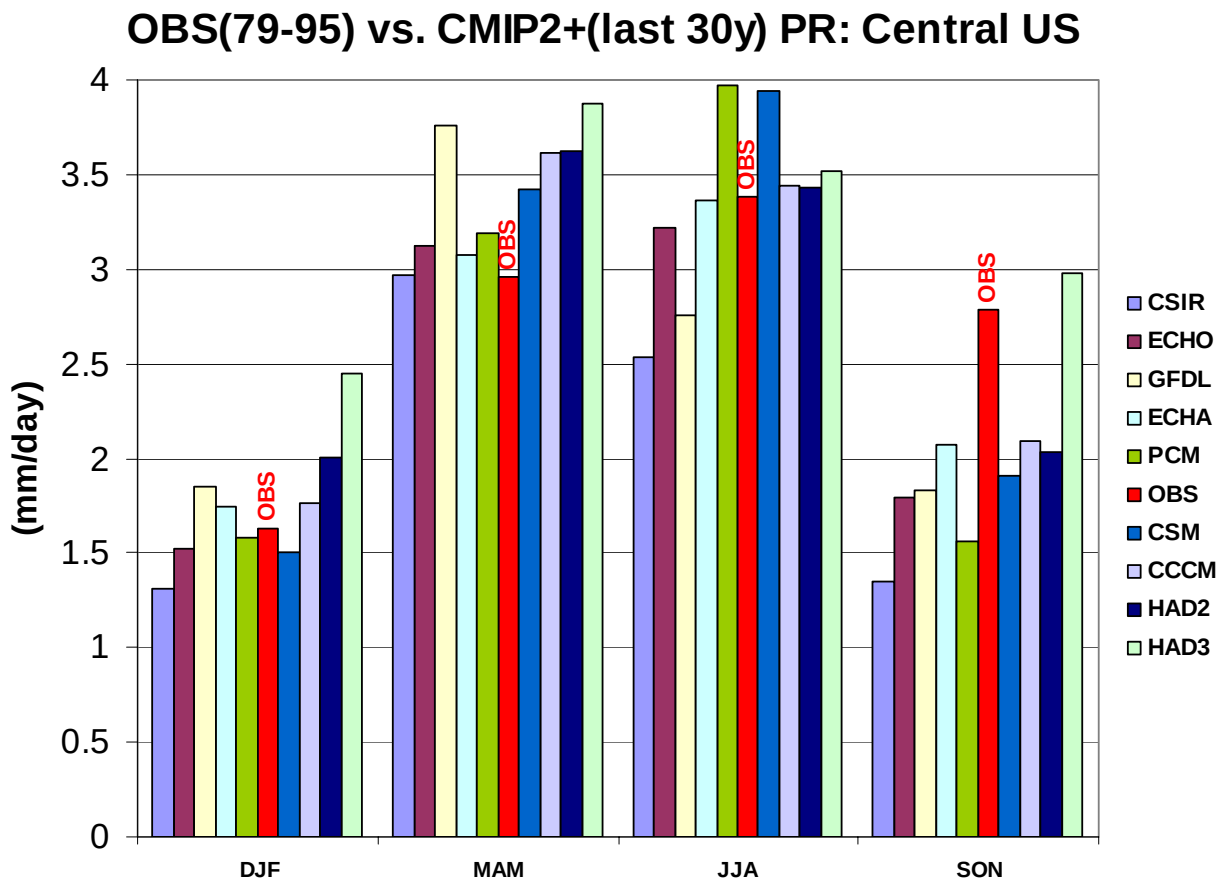

Fig. 20. Seasonal precipitation for the observations (1979-1995) and the control runs of the CMIP models.

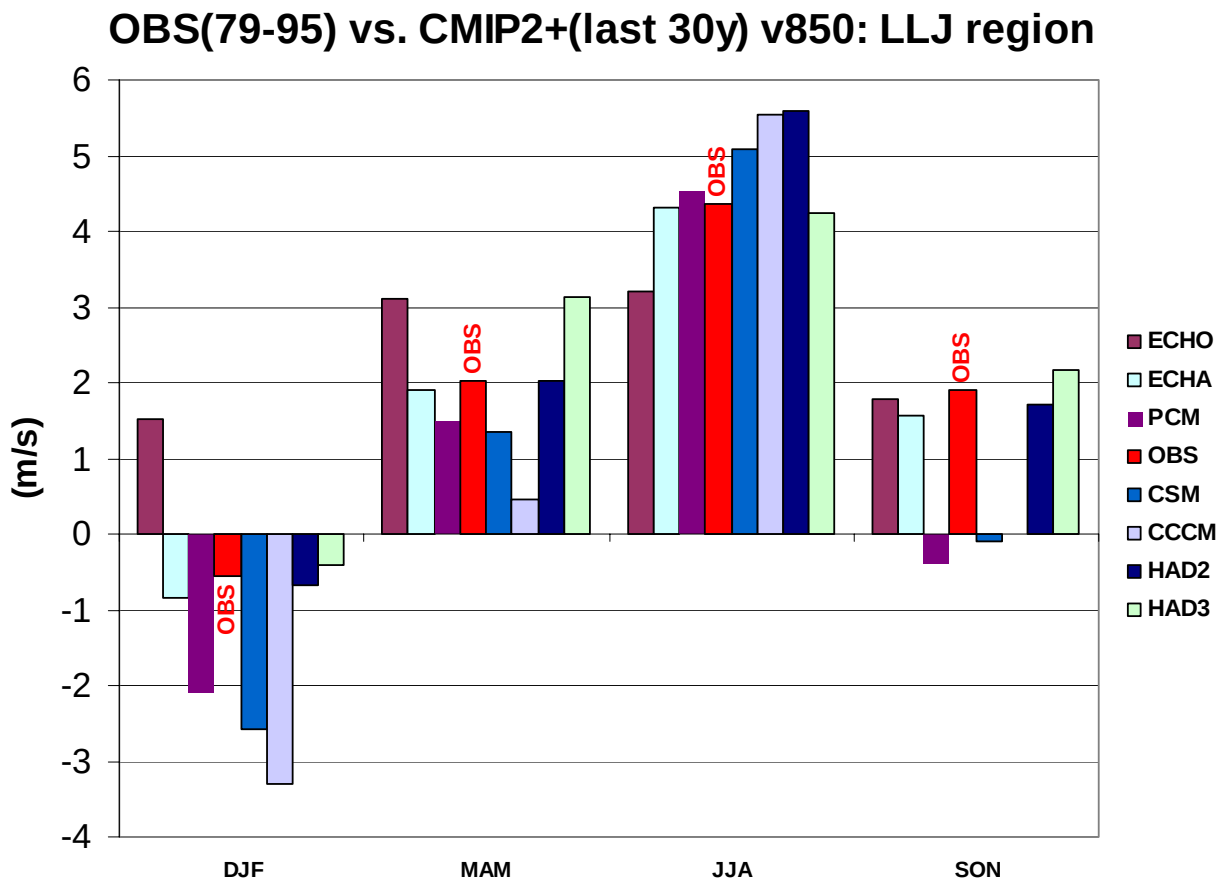

Figure 21. Southerly wind component (m s^{-1}) at 850 hPa in the LLJ region for the 4 seasons for CMIP models (last 30 years of control run) and observations for the period 1979-1995.

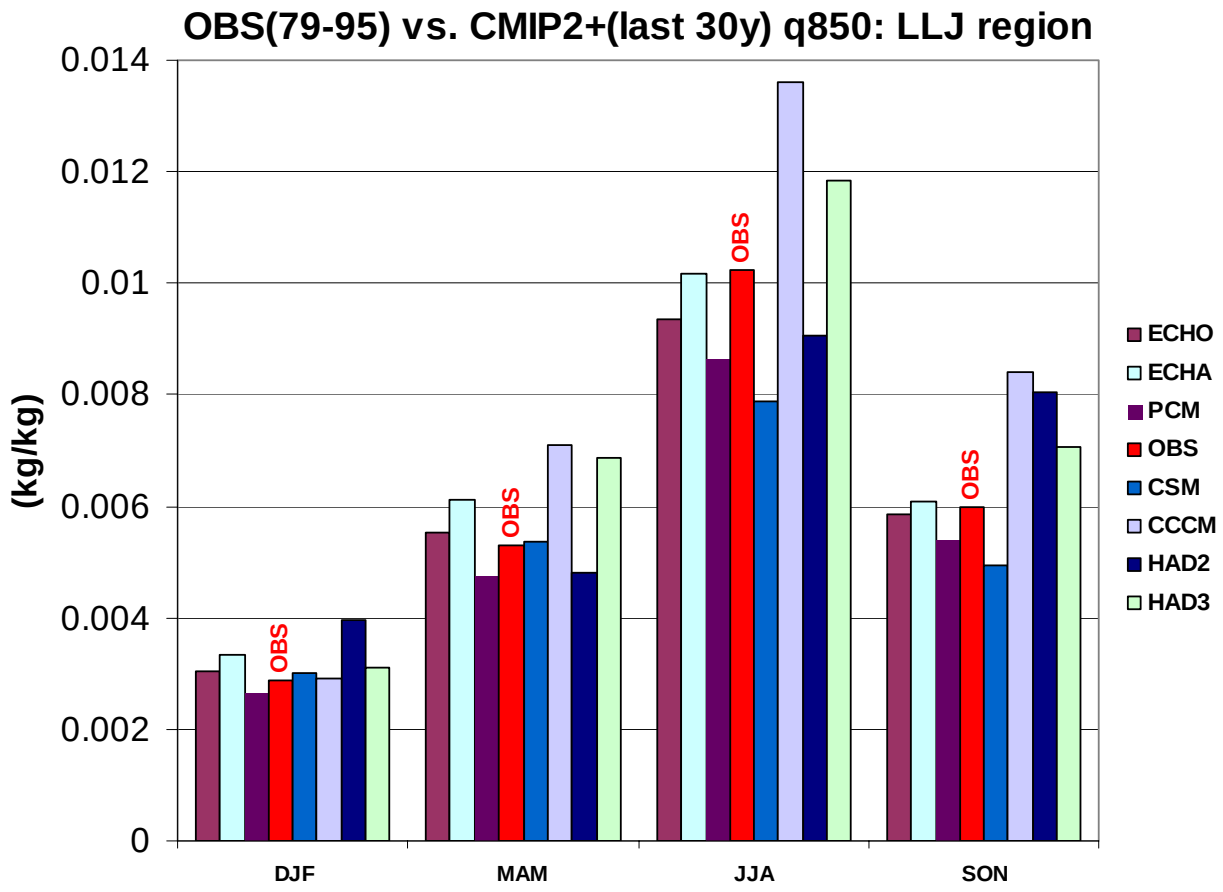

Fig. 22. Specific humidity at 850hPa of LLJ region for the four seasons for CMIP models (last 30 years of control run) and observations for the period 1979-1995.

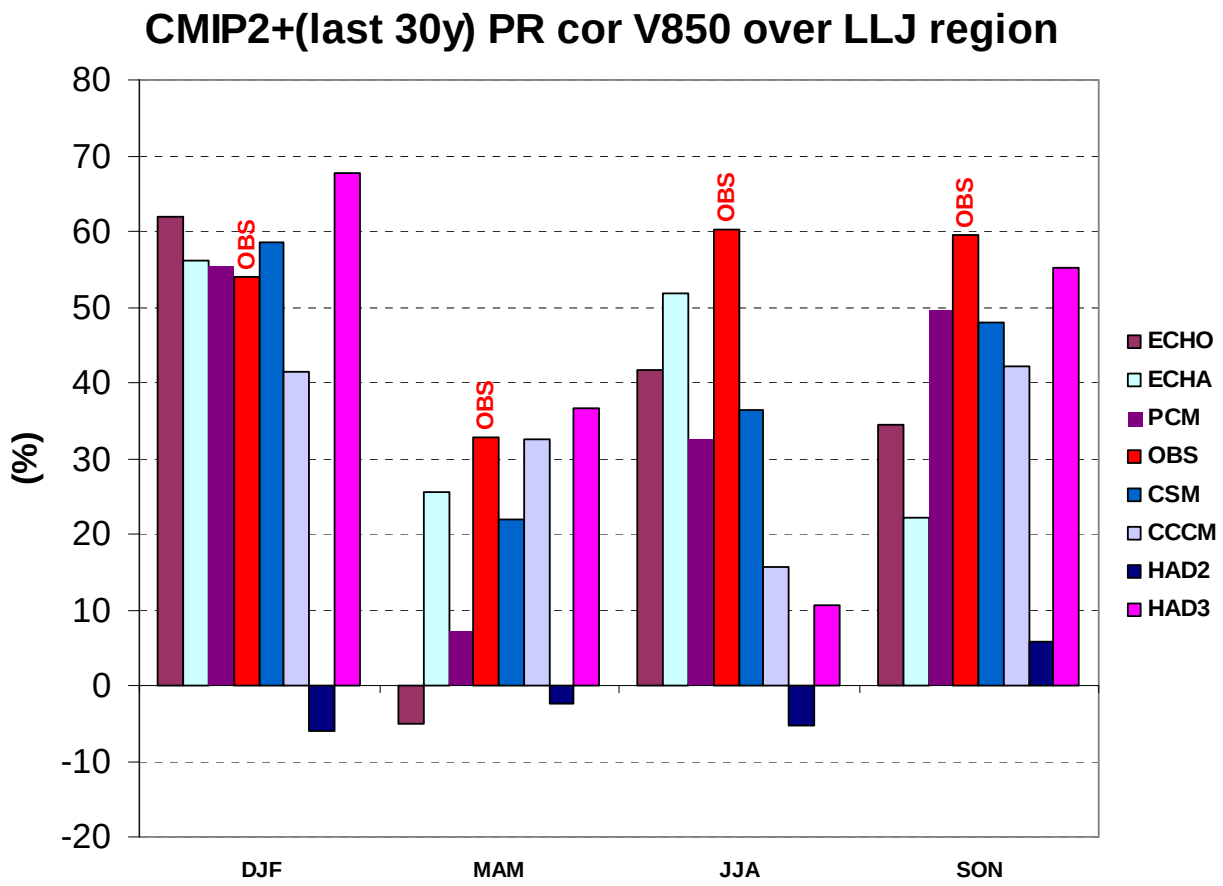

Fig. 23. Correlation between central US model precipitation and model southerly wind component in the LLJ region for CMIP models by season.

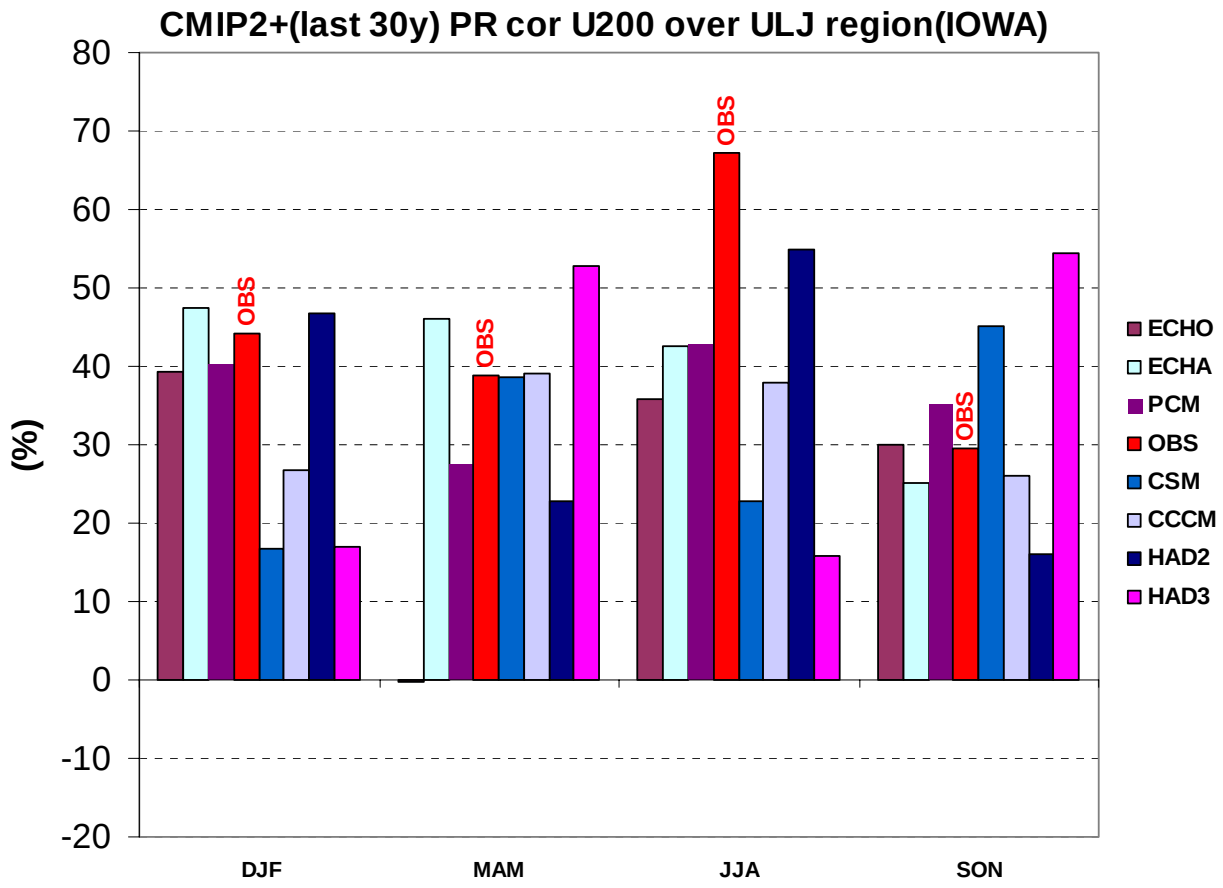

Fig. 24. Correlation coefficient for 4 seasons for CMIP models between model precipitation in the central U.S. and model westerly component of the wind speed at 200 hPa in the Iowa region (Fig. 13).

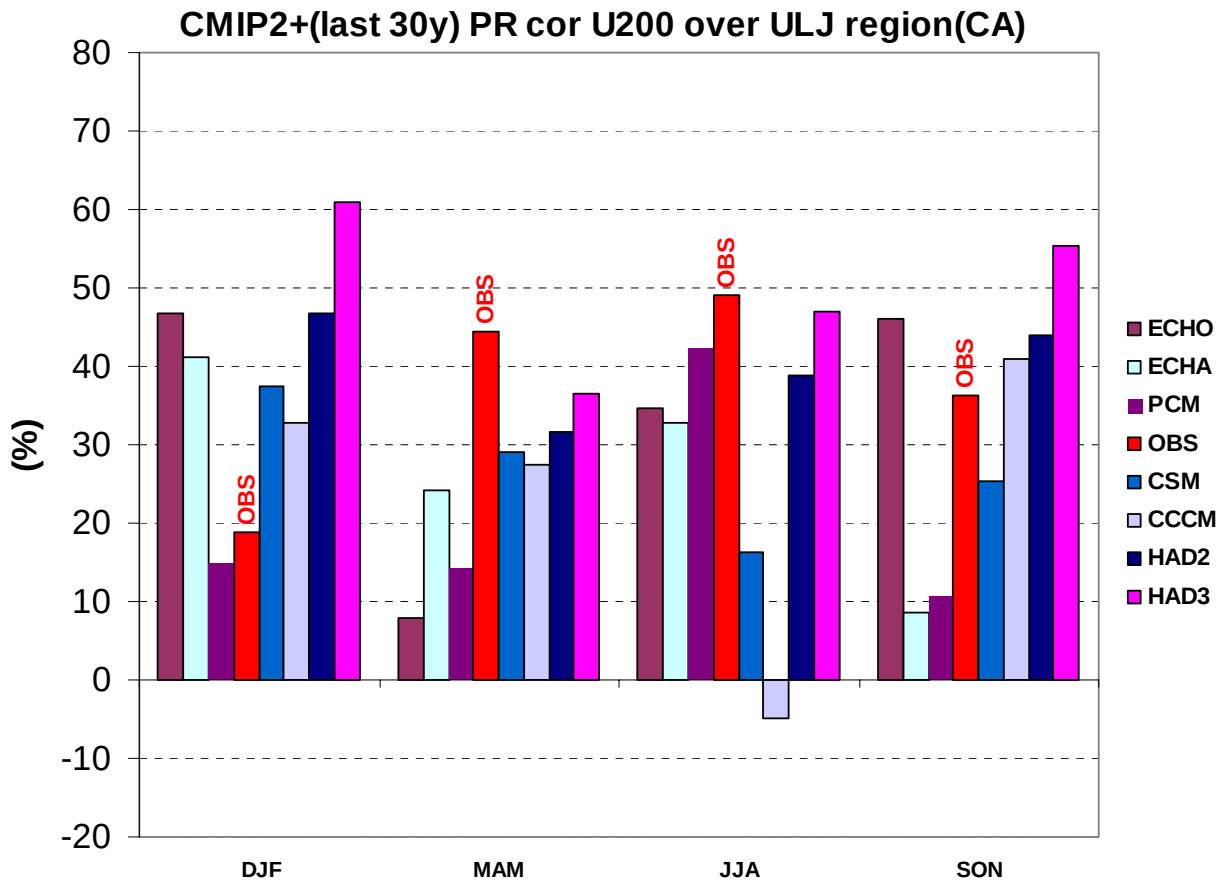

Figure 25. Correlation coefficient for 4 seasons for CMIP models between model precipitation in the central U.S. and model westerly component of the wind speed at 200 hPa in the California region (Fig. 13).

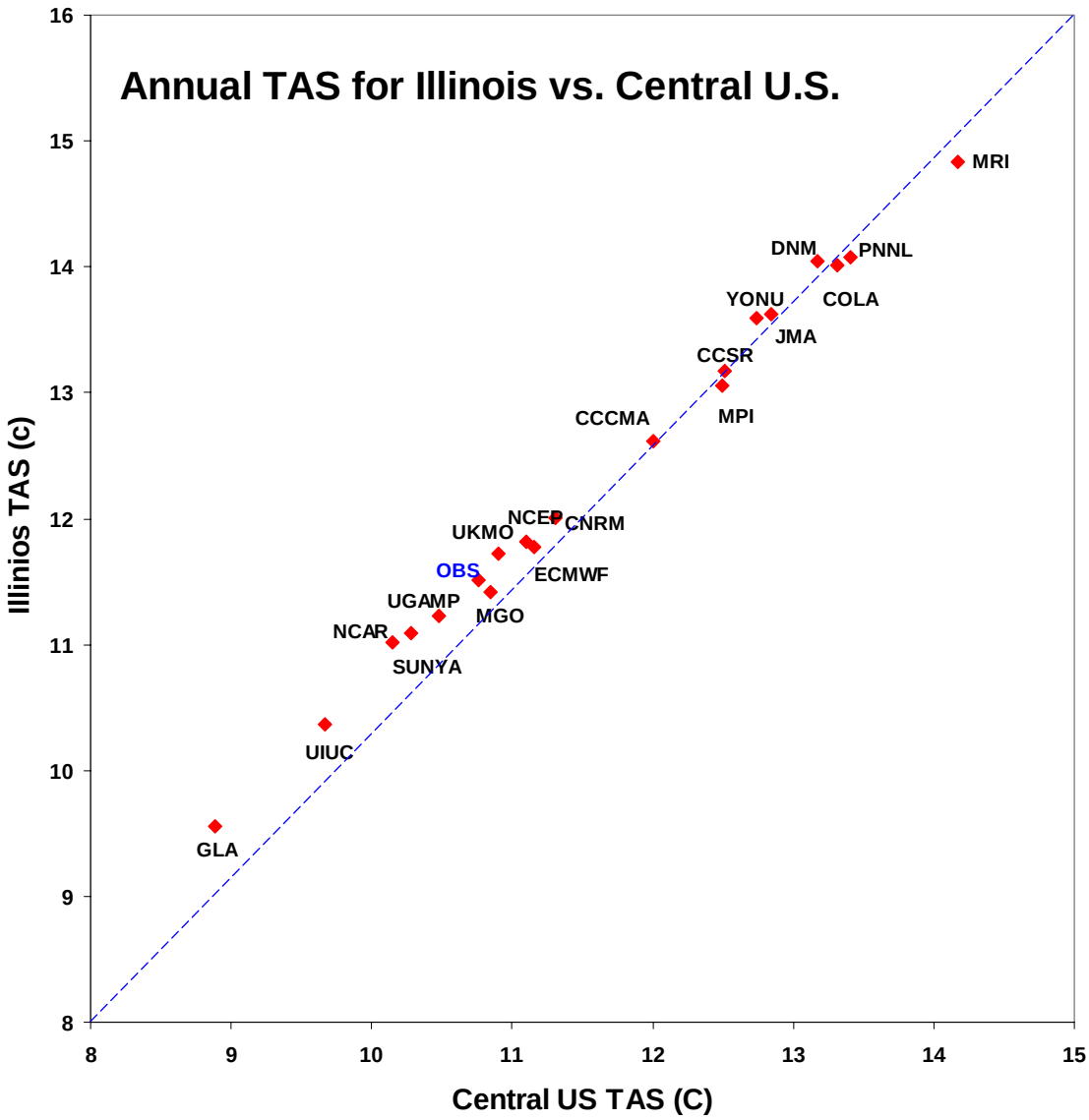

Figure 26 Annual surface air temperature for Illinois versus annual surface air temperature for central U.S. Units are °C. Each point represents a different AMIP model.

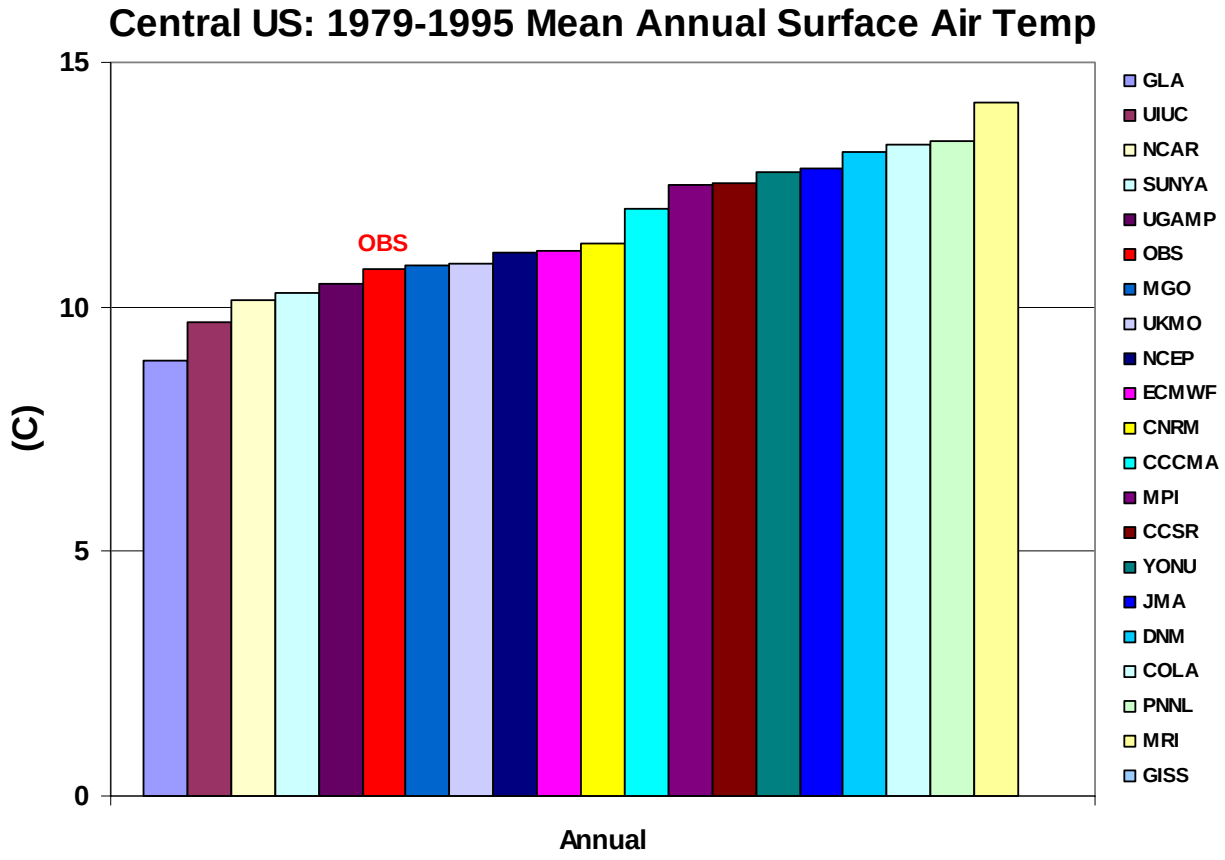

Figure 27 Annual surface air temperature (°C) for the central U.S. for AMIP models and observations. AMIP model values are plotted in order of increasing temperature. The period covered is 1979-1995.

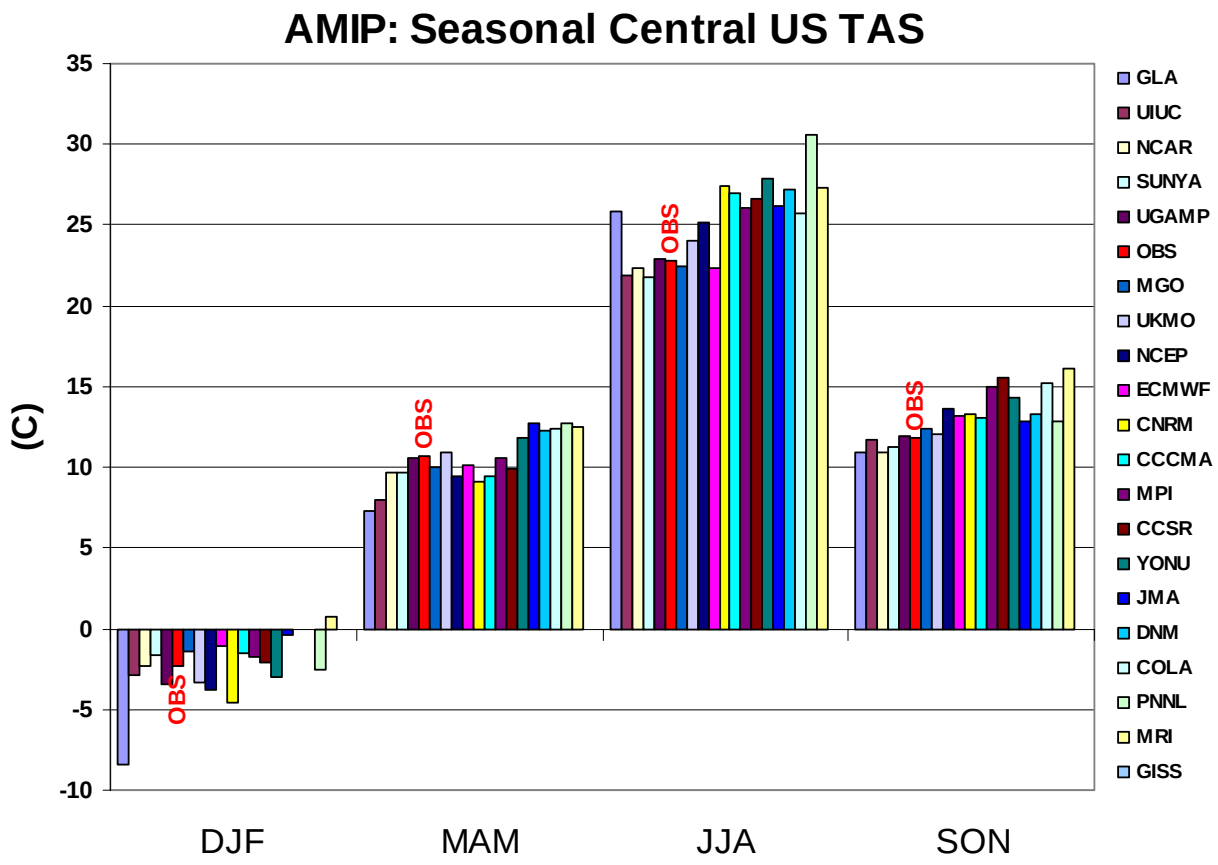

Figure 28 Seasonal (winter, spring, summer, fall) central U.S. surface air temperature (°C) for AMIP models and observations for the period 1979-1995.

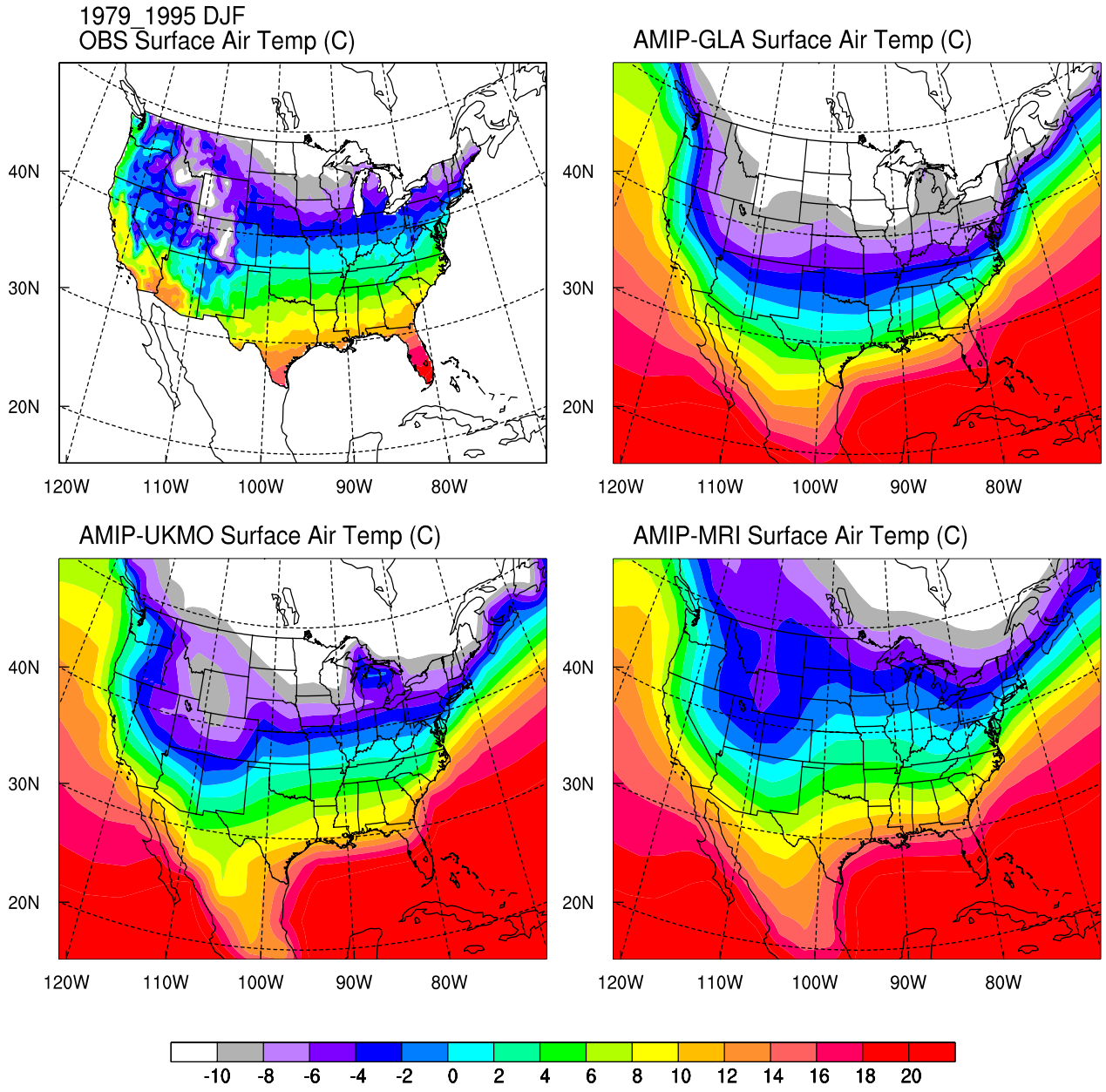

Figure 29. Maps of winter surface air temperature (°C) from observations (top left), the GLA (coldest annual) model (top right), the UKMO (an intermediate) model (bottom left), and the MRI (warmest) model (bottom right).

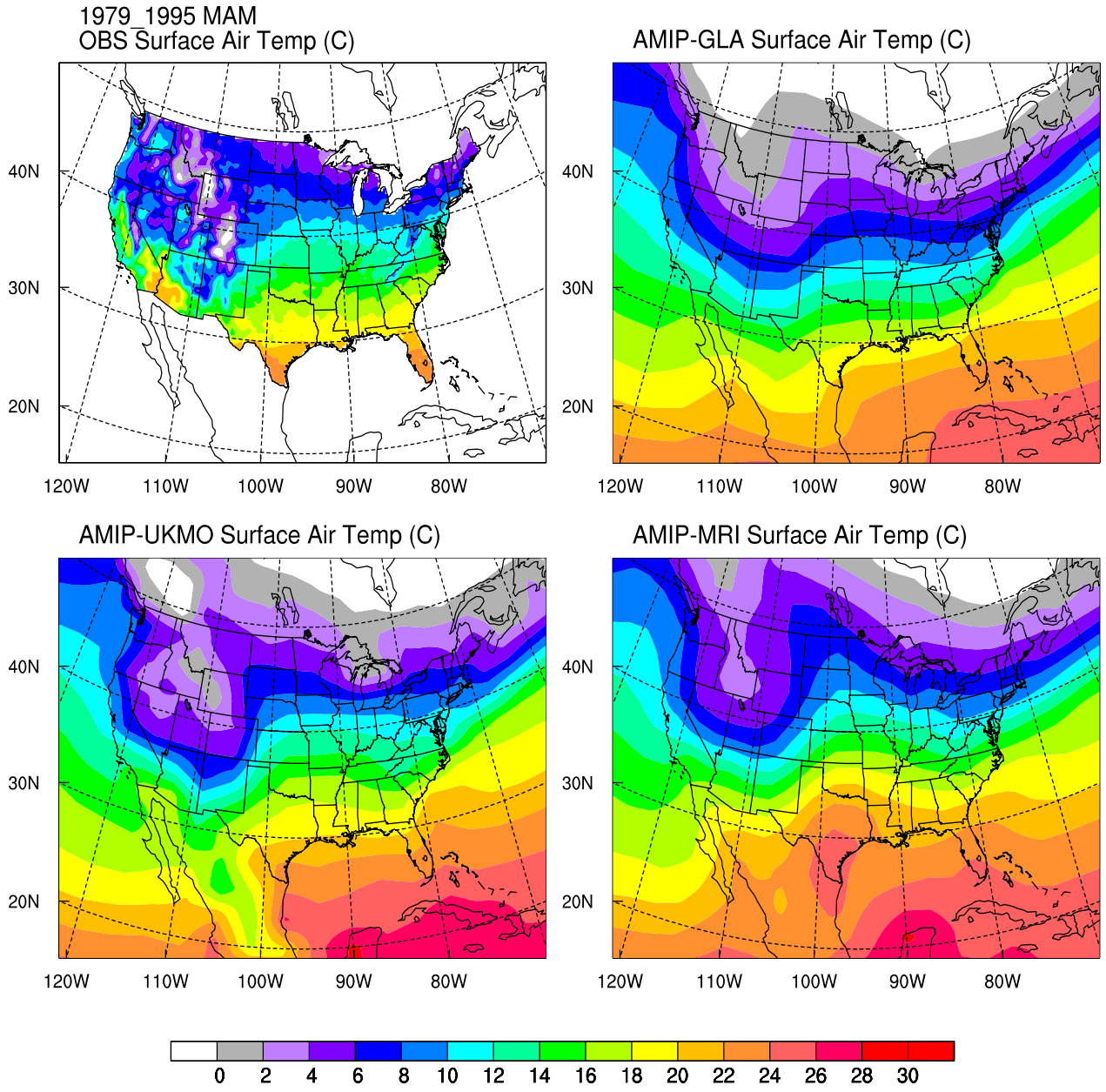

Figure 30. Maps of spring surface air temperature (°C) from observations (top left), the GLA (coldest annual) model (top right), the UKMO (an intermediate) model (bottom left), and the MRI (warmest) model (bottom
right).

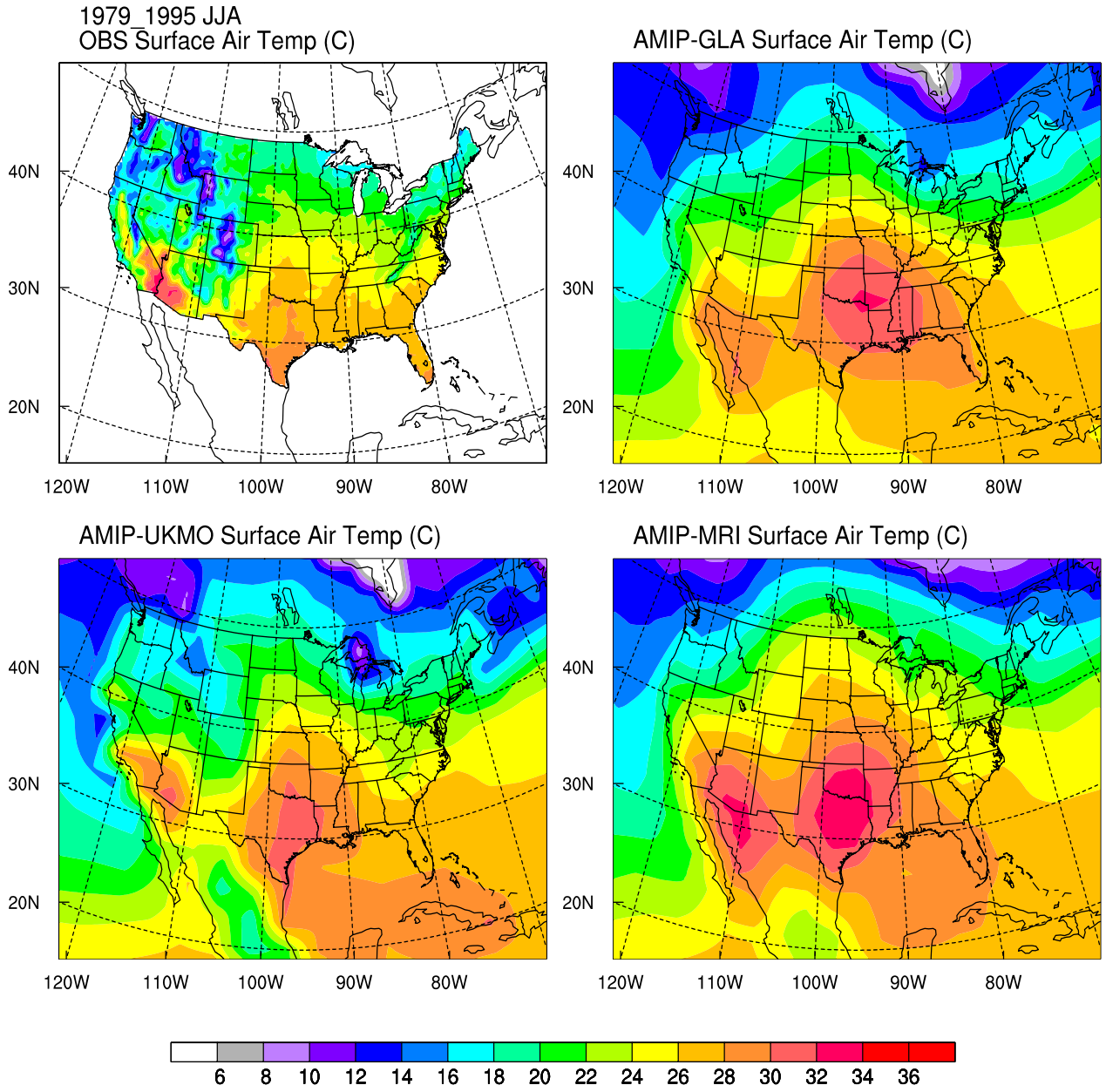

Figure 31. Maps of summer surface air temperature (°C) from observations (top left), the GLA (coldest annual) model (top right), the UKMO (an intermediate) model (bottom left), and the MRI (warmest) model (bottom right).

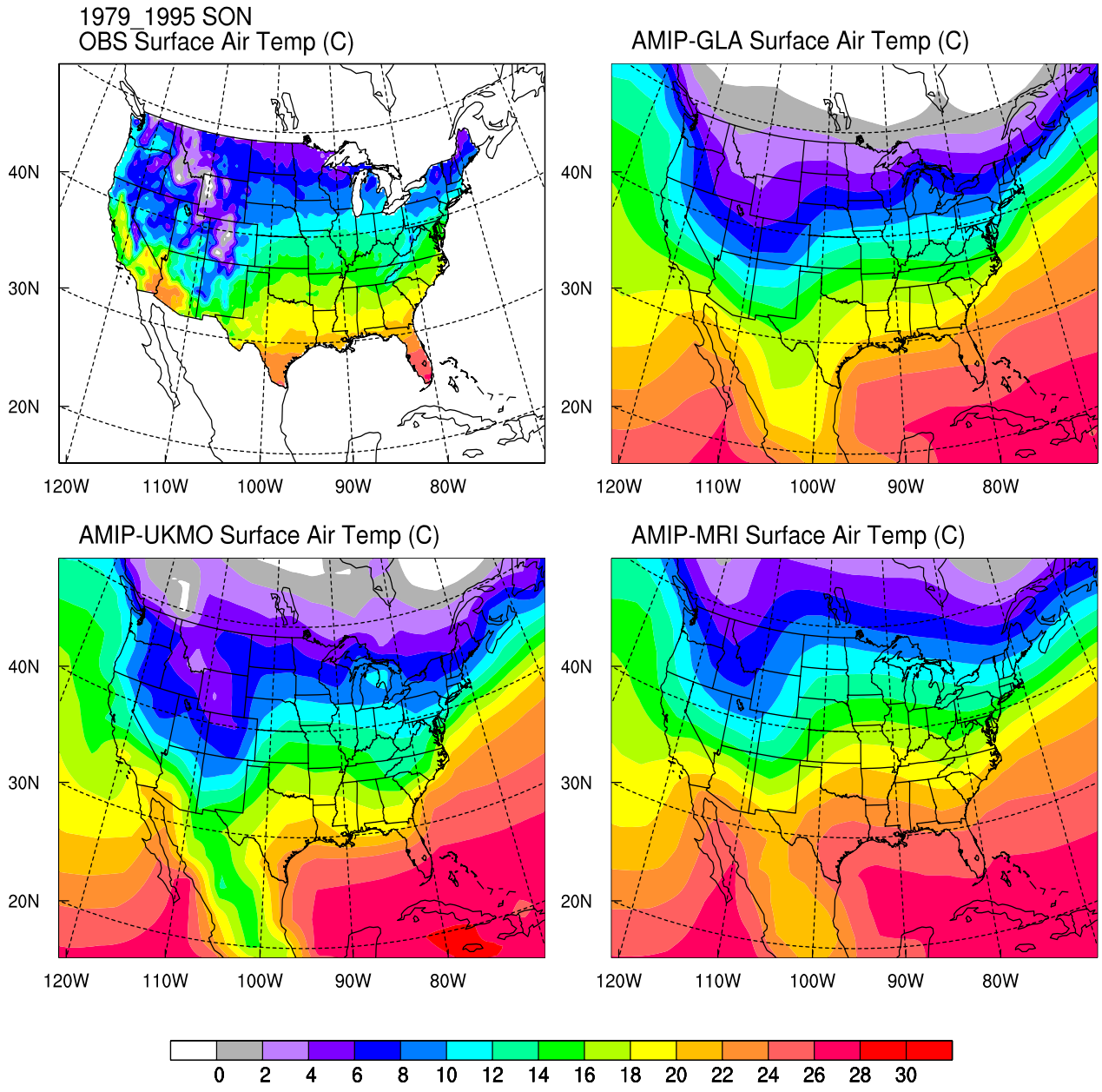

Figure 32. Maps of fall surface air temperature (°C) from observations (top left), the GLA (coldest annual) model (top right), the UKMO (an intermediate) model (bottom left), and the MRI (warmest) model (bottom right).

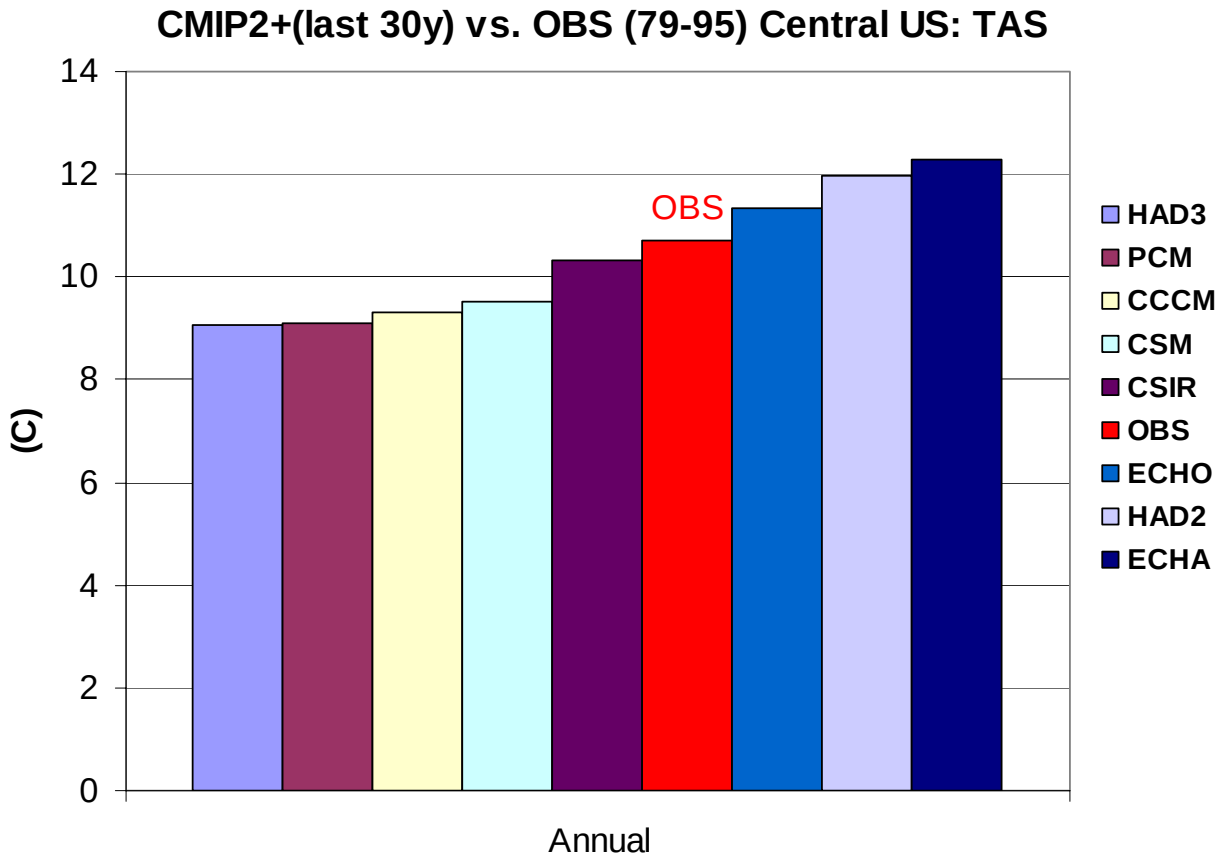

Fig. 33. Annual surface air temperature (°C) for the central U.S. for CMIP models and observations. The CMIP values were obtained from an average of the last 30 years of each model's control run. The observed value is for the period 1979-1995.

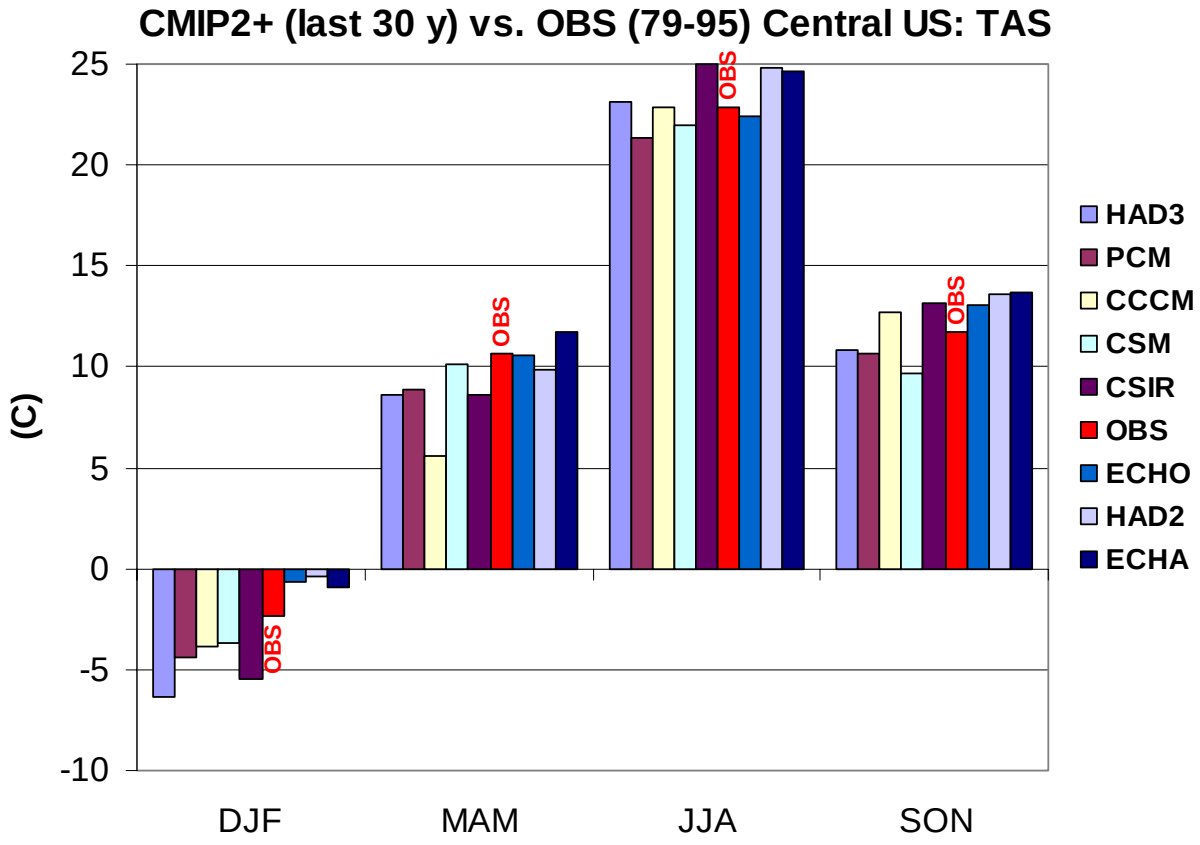

Figure 34. Seasonal mean surface air temperature (°C) for the central U.S. for CMIP models and observations. The CMIP values were obtained from an average of the last 30 years of each model's control run. The observed value is for the period 1979-1995.

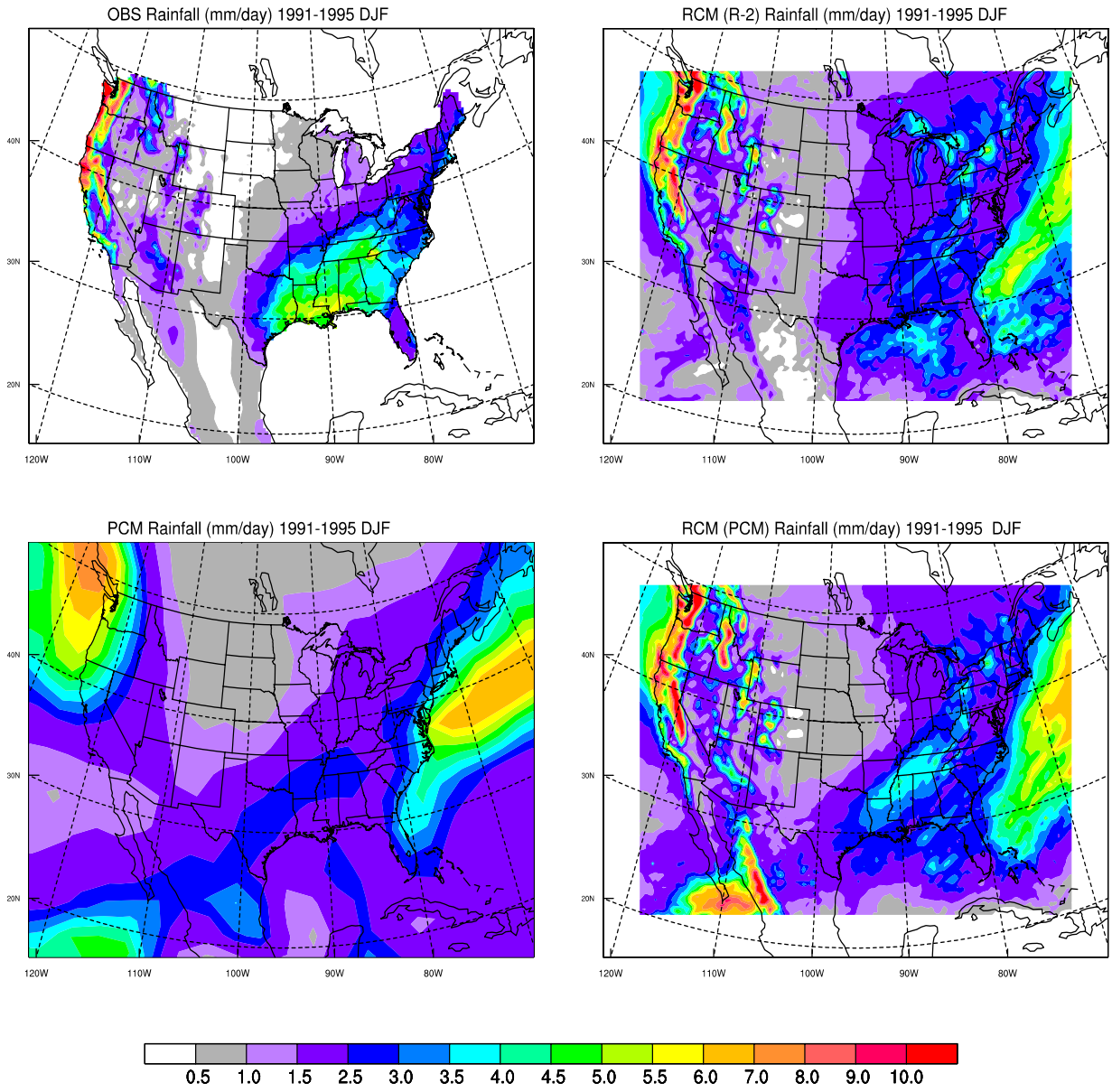

Figure 35. Maps of winter precipitation (mm d^{-1}) for 1991-1995 from observations (top left), RCM driven by the reanalysis data (R-2) (top right), the Parallel Climate Model (PCM) (bottom left), and the RCM driven by the PCM (bottom right).

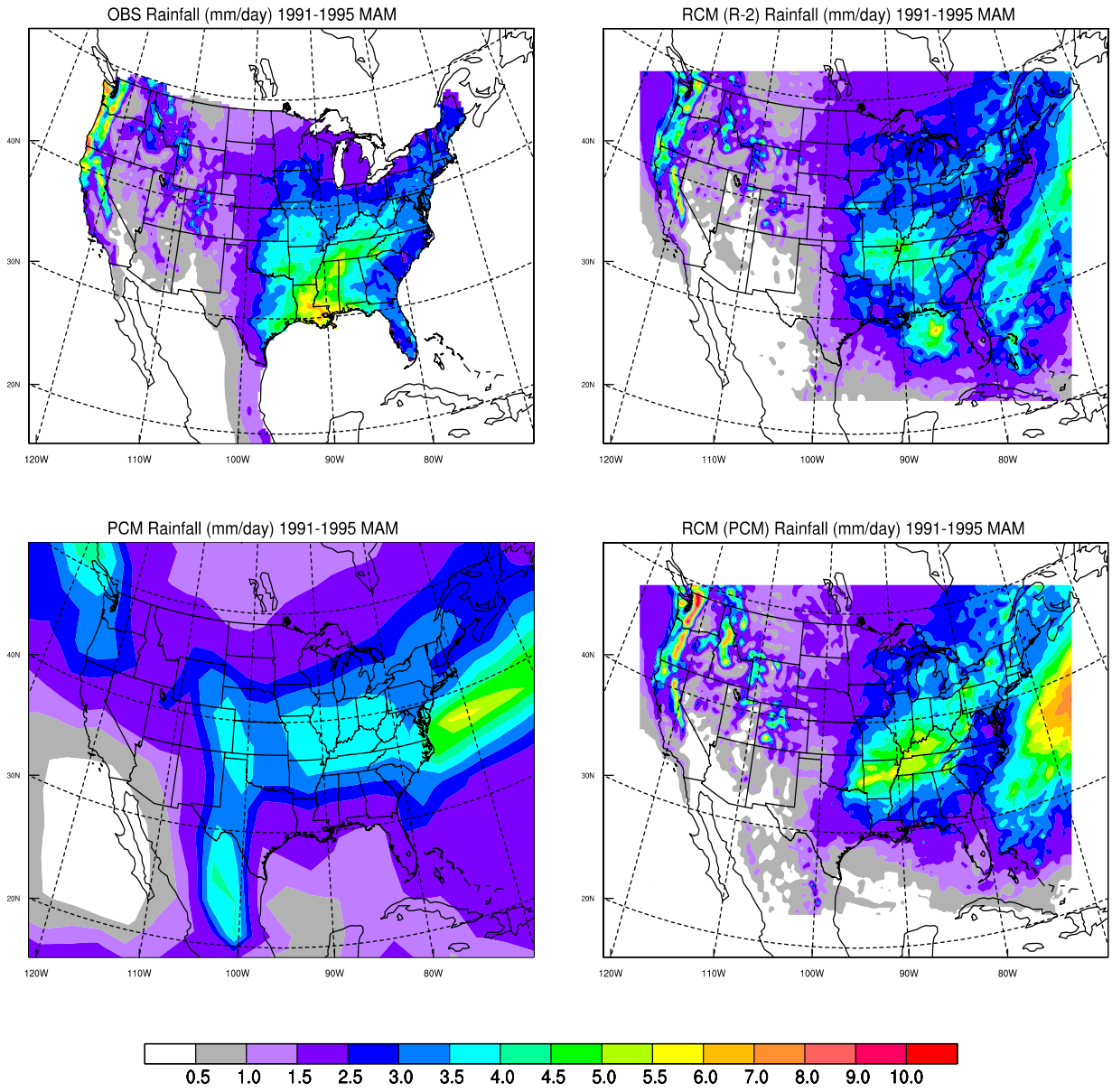

Figure 36. Maps of spring precipitation (mm d^{-1}) for 1991-1995 from observations (top left), RCM driven by the reanalysis data (R-2) (top right), the Parallel Climate Model (PCM) (bottom left), and the RCM driven by the PCM (bottom right).

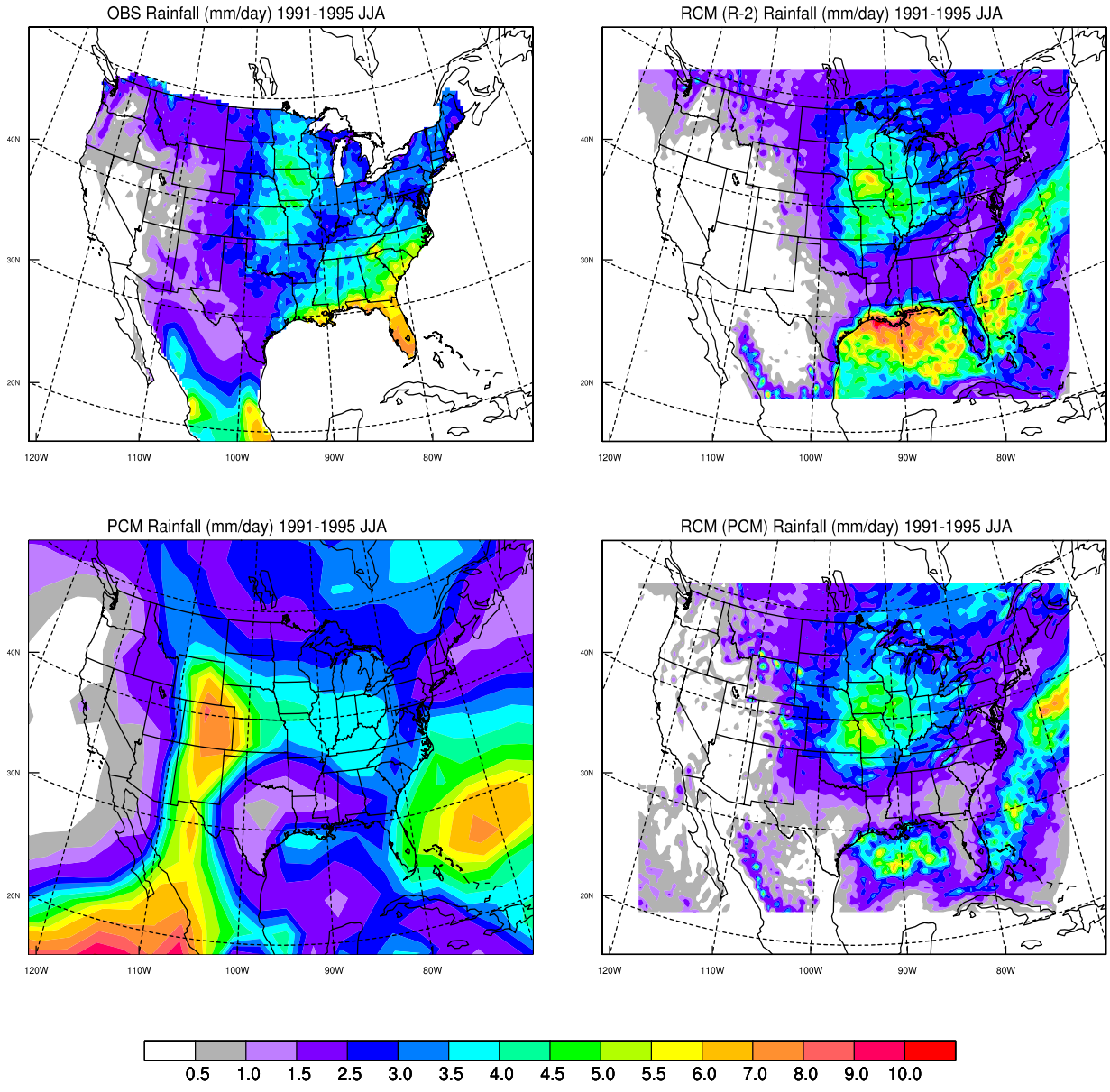

Figure 37. Maps of summer precipitation (mm d^{-1}) for 1991-1995 from observations (top left), RCM driven by the reanalysis data (R-2) (top right), the Parallel Climate Model (PCM) (bottom left), and the RCM driven by the PCM (bottom right).

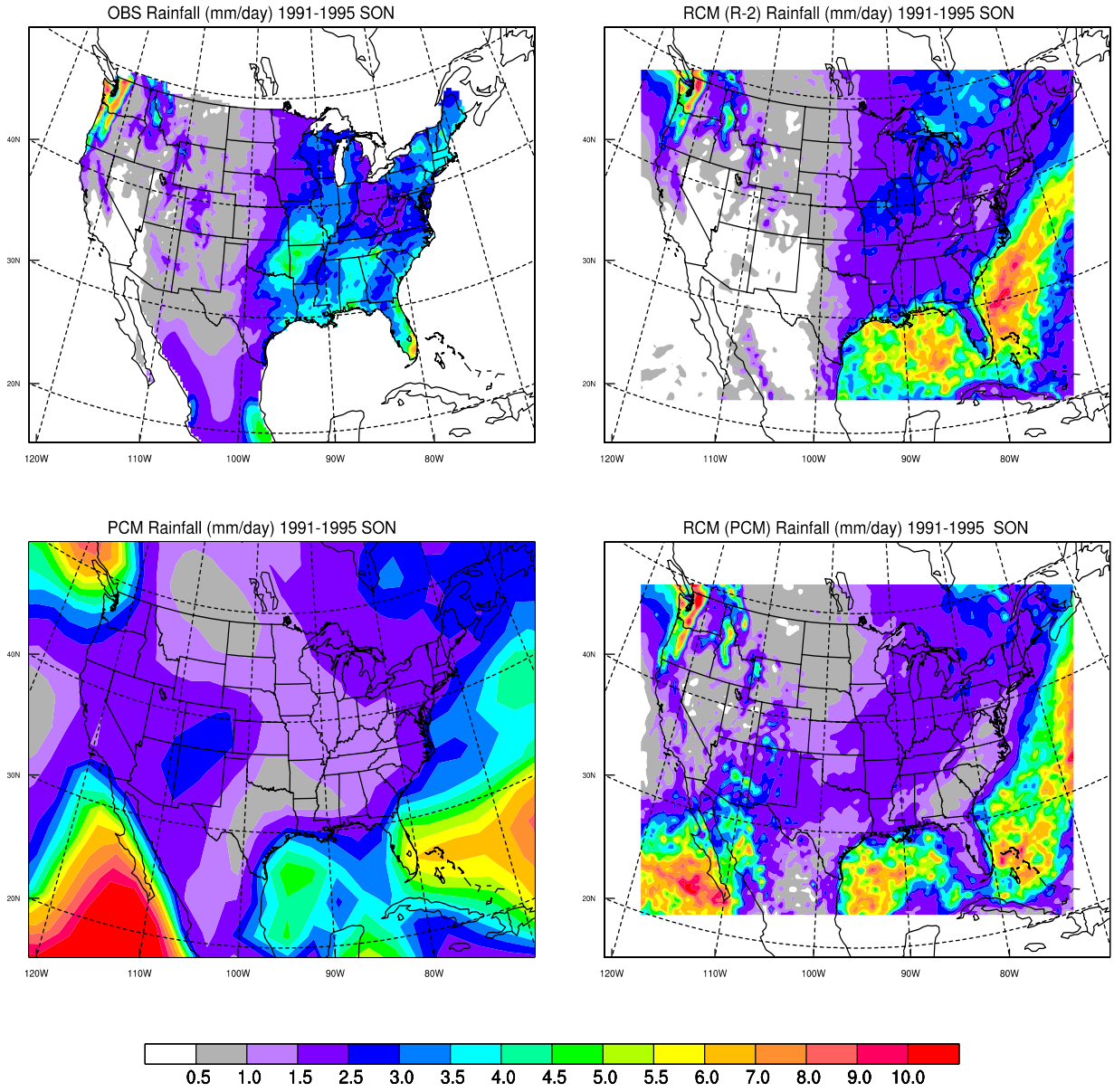

Figure 38. Maps of fall precipitation (mm d^{-1}) for 1991-1995 from observations (top left), RCM driven by the reanalysis data (R-2) (top right), the Parallel Climate Model (PCM) (bottom left), and the RCM driven by the PCM (bottom right).

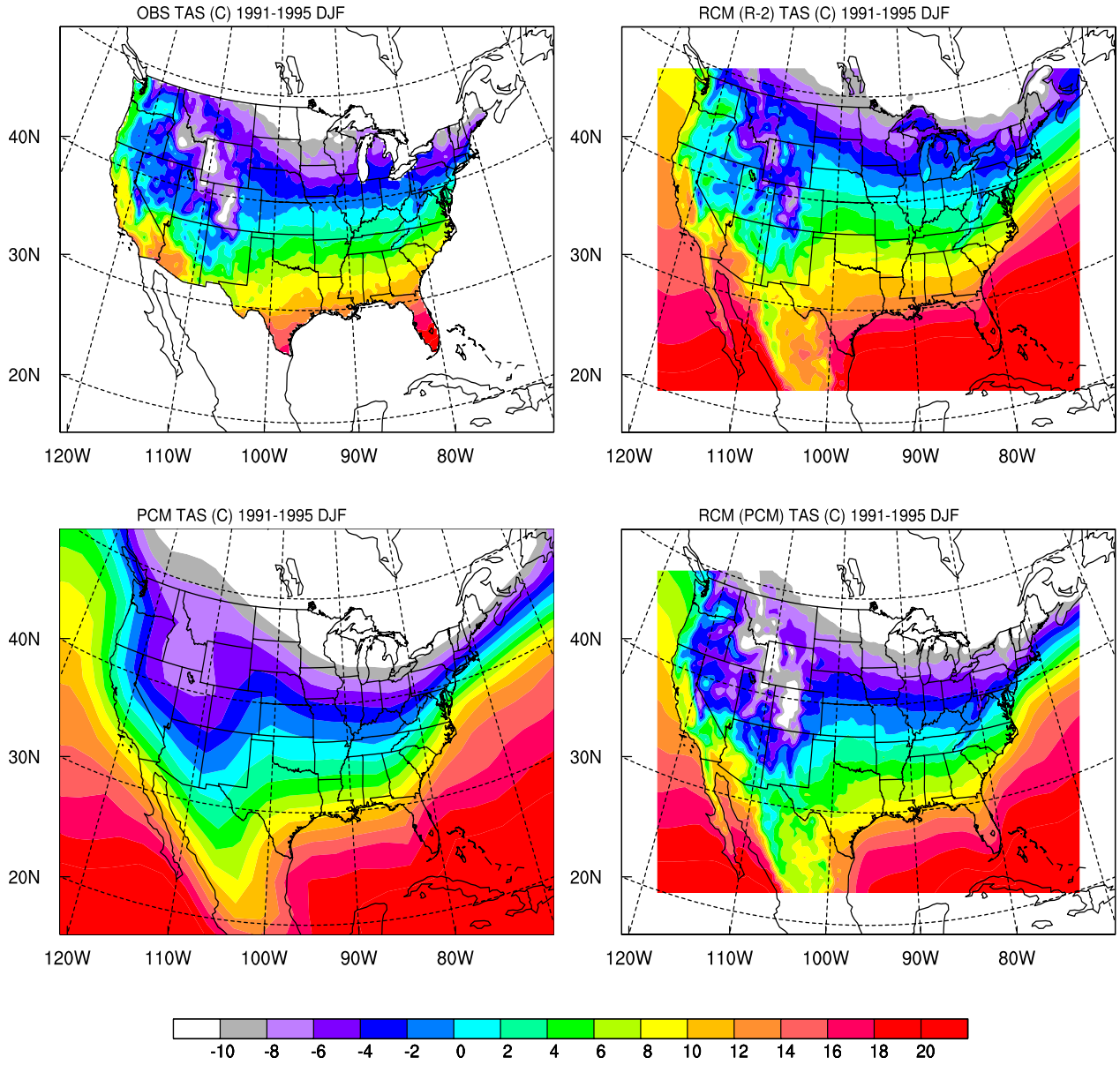

Figure 39. Maps of winter surface air temperature (°C) for 1991-1995 from observations (top left), RCM driven by the reanalysis data (R-2) (top right), the Parallel Climate Model (PCM) (bottom left), and the RCM driven by the PCM (bottom right).

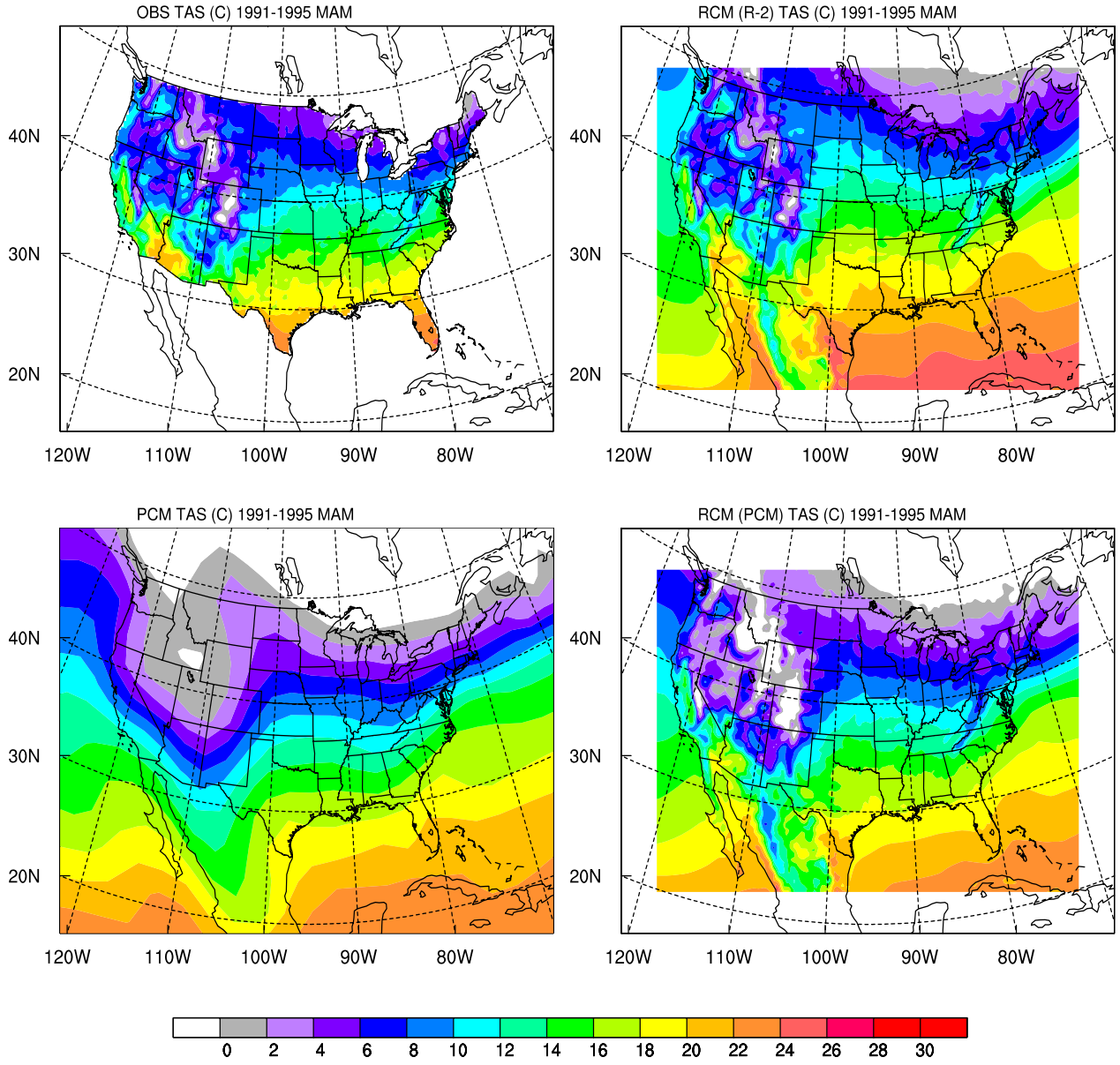

Figure 40. Maps of spring surface air temperature (°C) for 1991-1995 from observations (top left), RCM driven by the reanalysis data (R-2) (top right), the Parallel Climate Model (PCM) (bottom left), and the RCM driven by the PCM (bottom right).

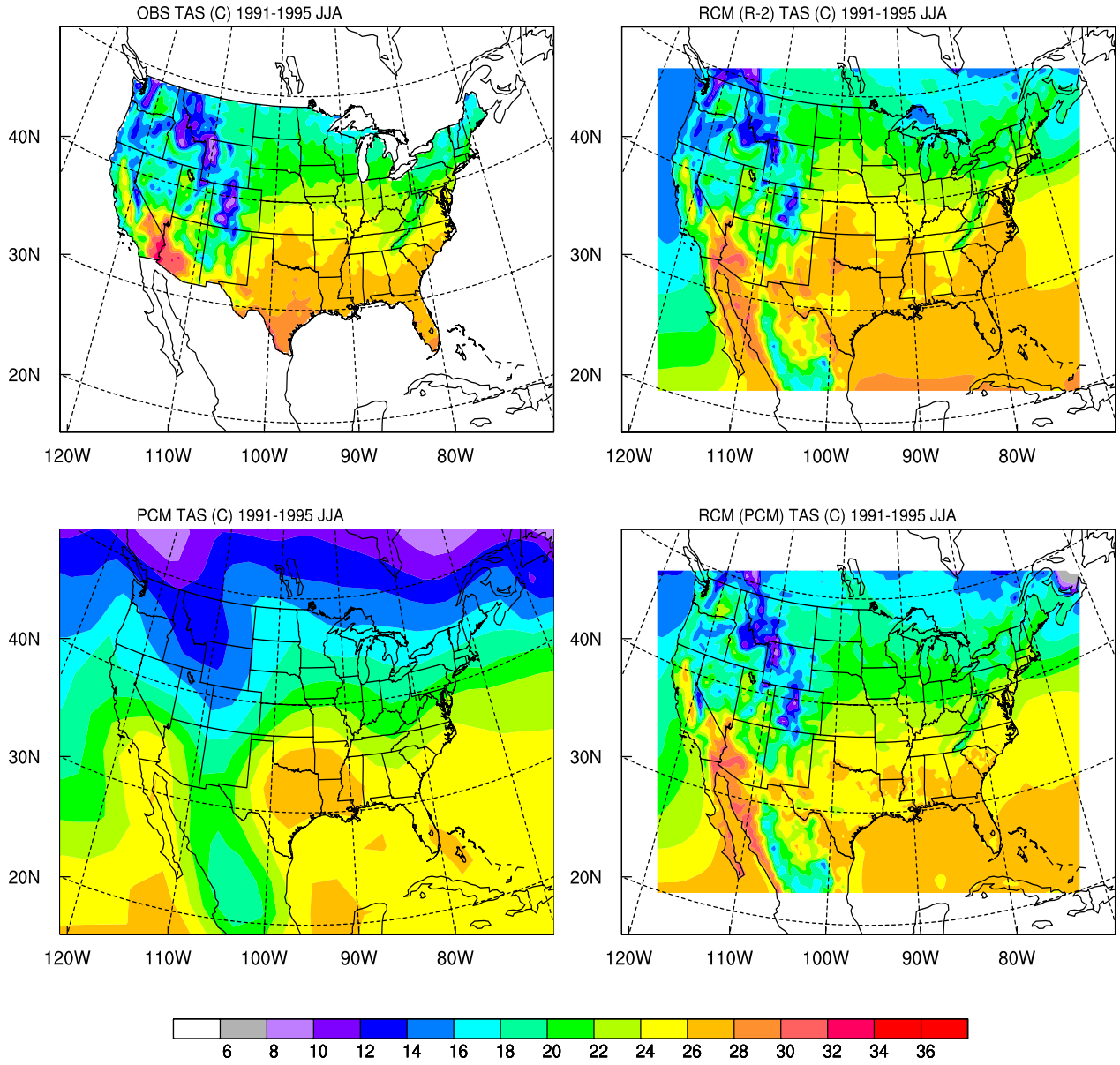

Figure 41. Maps of summer surface air temperature (°C) for 1991-1995 from observations (top left), RCM driven by the reanalysis data (R-2) (top right), the Parallel Climate Model (PCM) (bottom left), and the RCM driven by the PCM (bottom right).

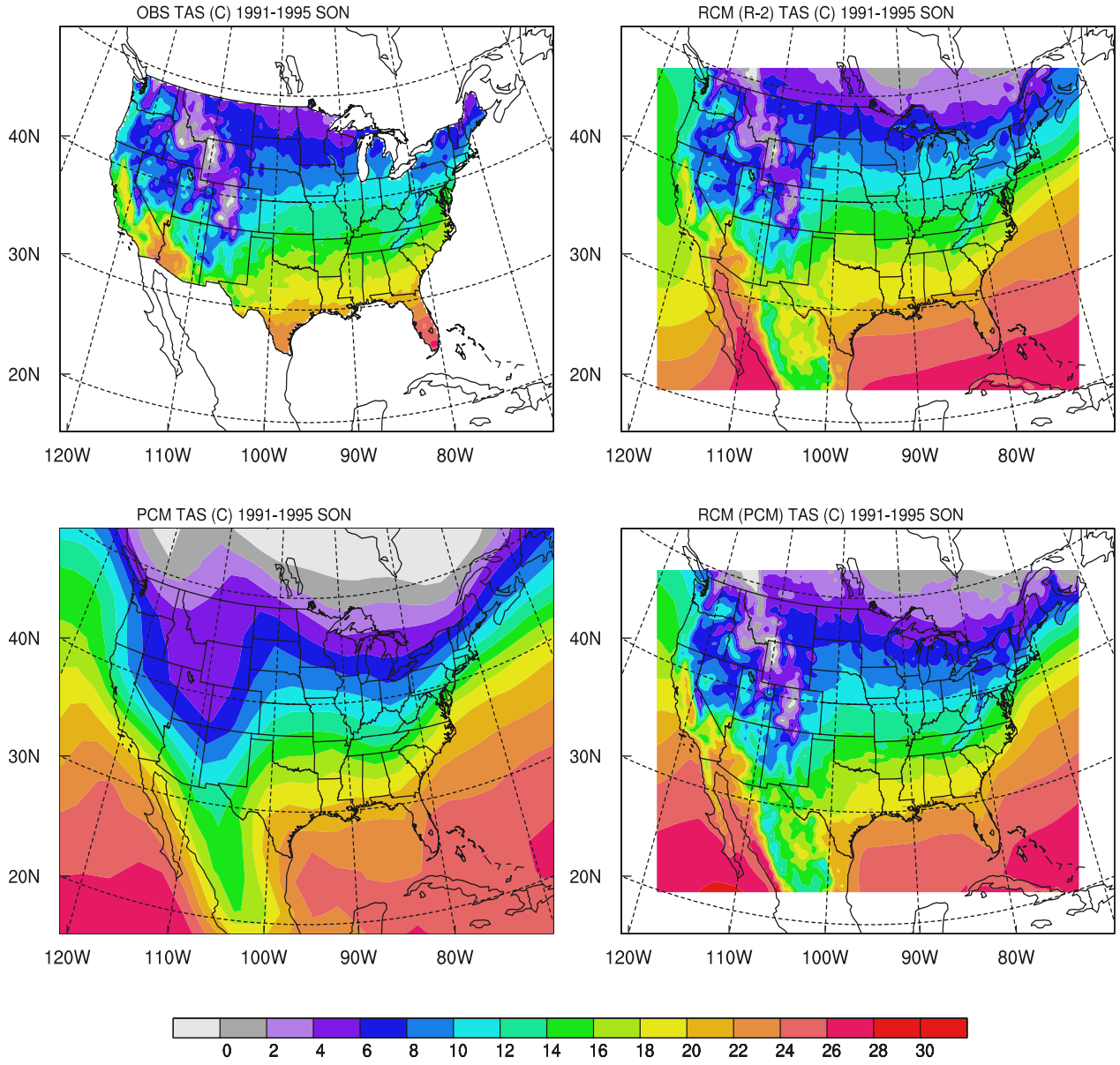

Figure 42. Maps of fall surface air temperature (°C) for 1991-1995 from observations (top left), RCM driven by the reanalysis data (R-2) (top right), the Parallel Climate Model (PCM) (bottom left), and the RCM driven by the PCM (bottom right).

:

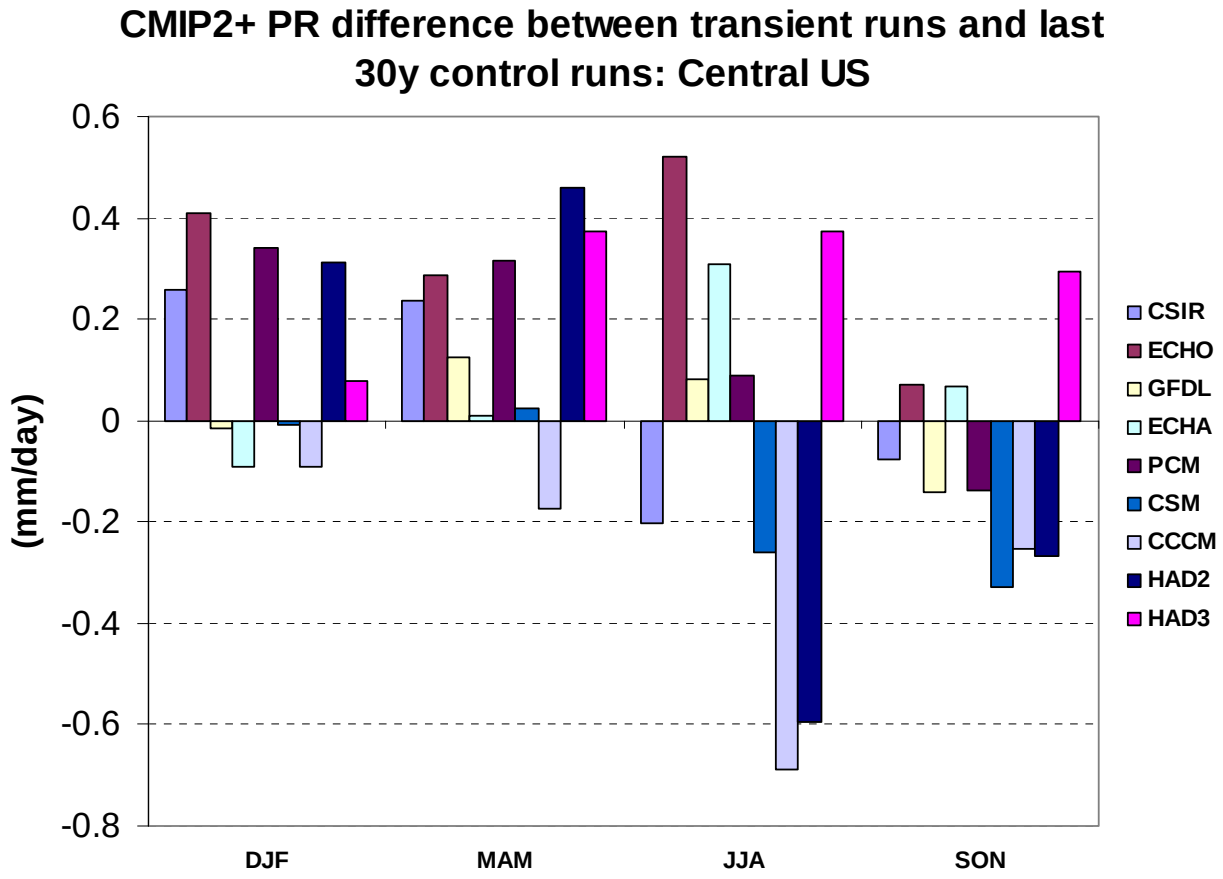

Figure 43. Precipitation changes in the transient runs of the CMIP models for the central U.S. The change is the difference between the average of years 65-75 in the transient run and the average of the last 30 years of the control run.

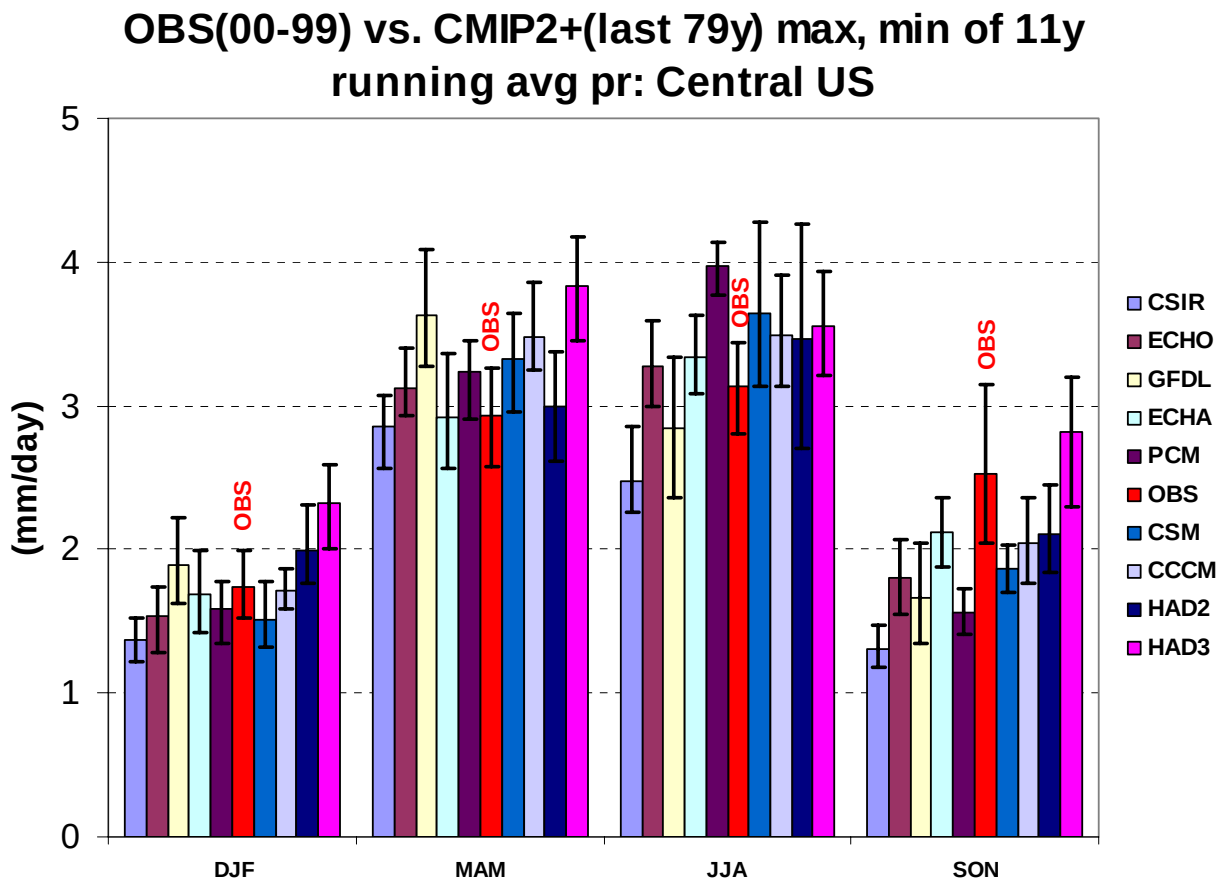

Figure 44. The mean, maximum, and minimum values of a 11-year running average of the control run and mean, maximum, and minimum values of a 11-yr running average of the 20th Century (1900-1999) observations for central US precipitation for the four seasons. The mean is indicated by the bar height while the maximum and minimum limits are denoted by the vertical line.

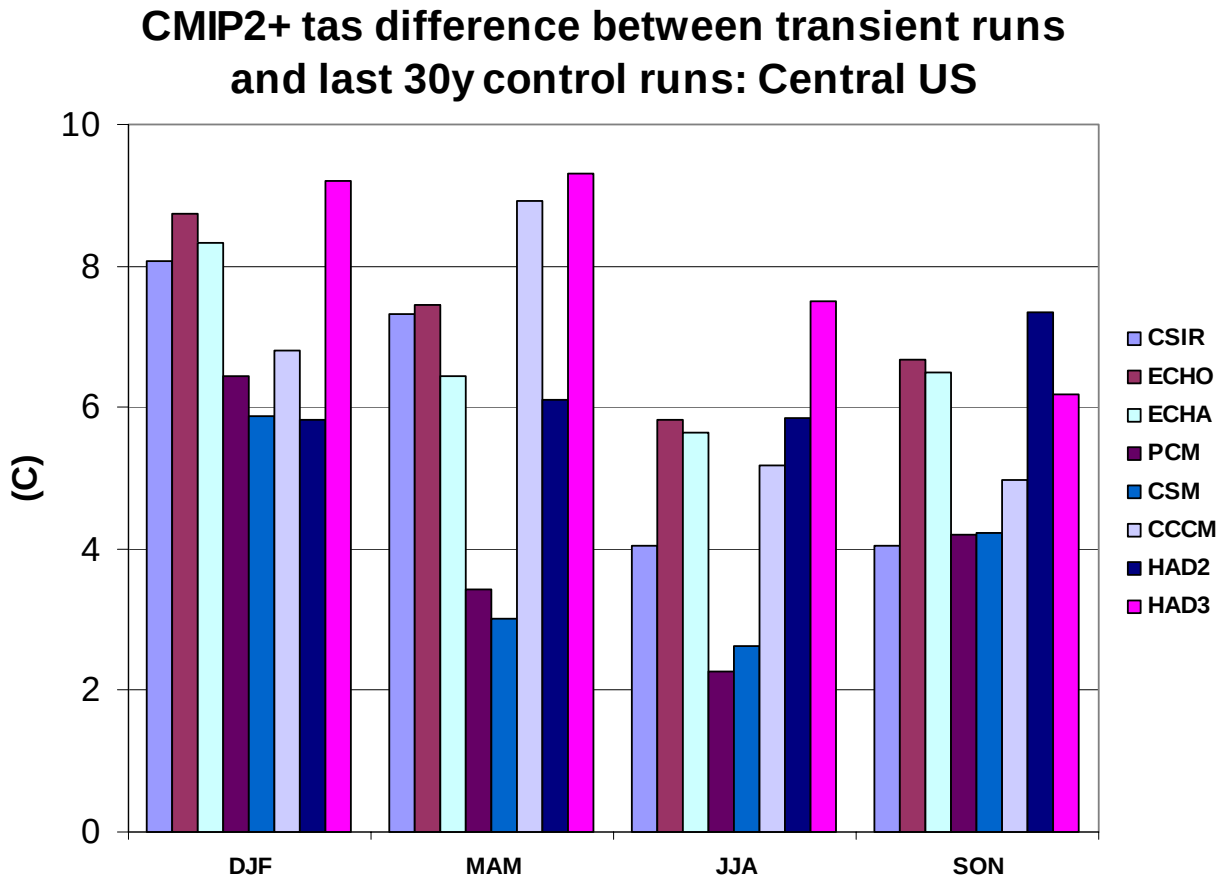

Fig. 45. Surface air temperature changes (°C) in the transient runs of the CMIP models for the central U.S. The change is the difference between the average of years 65-75 in the transient run and the average of the last 30 years of the control run.

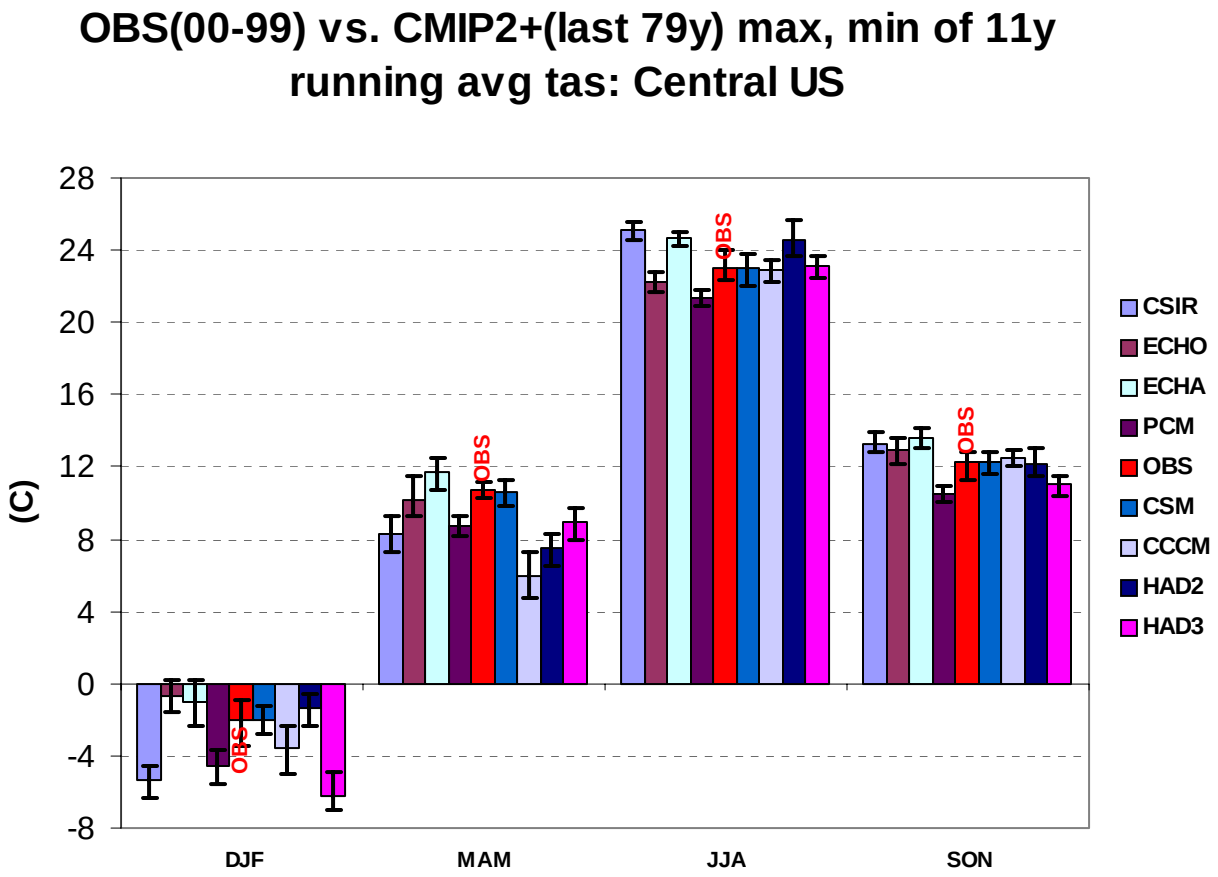

Figure 46. The mean, maximum, and minimum values of a 11-year running average of the control run and mean, maximum, and minimum values of a 11-yr running average of the 20th Century observations for central US surface air temperature for the four seasons. The mean is indicated by the bar height while the maximum and minimum limits are denoted by the vertical line.

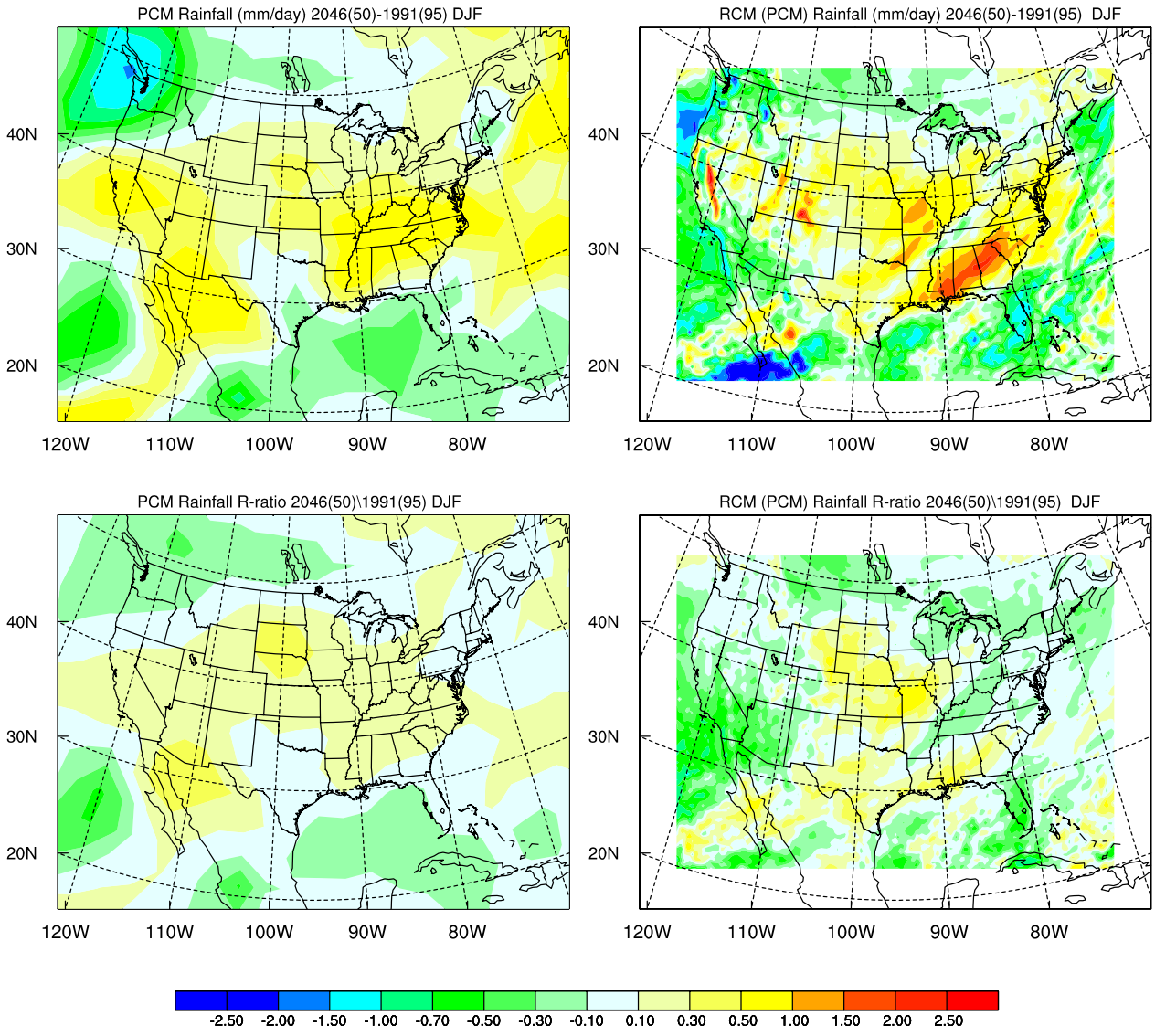

Figure 47. Maps of winter precipitation differences (2046-2050 minus 1991-1995) from (top and bottom left panels) the Parallel Climate Model and (top and bottom right panels) RCM driven by the PCM. Top panels show absolute differences (mm d-1) and bottom panels show these same differences expressed in percent of the PCM value.

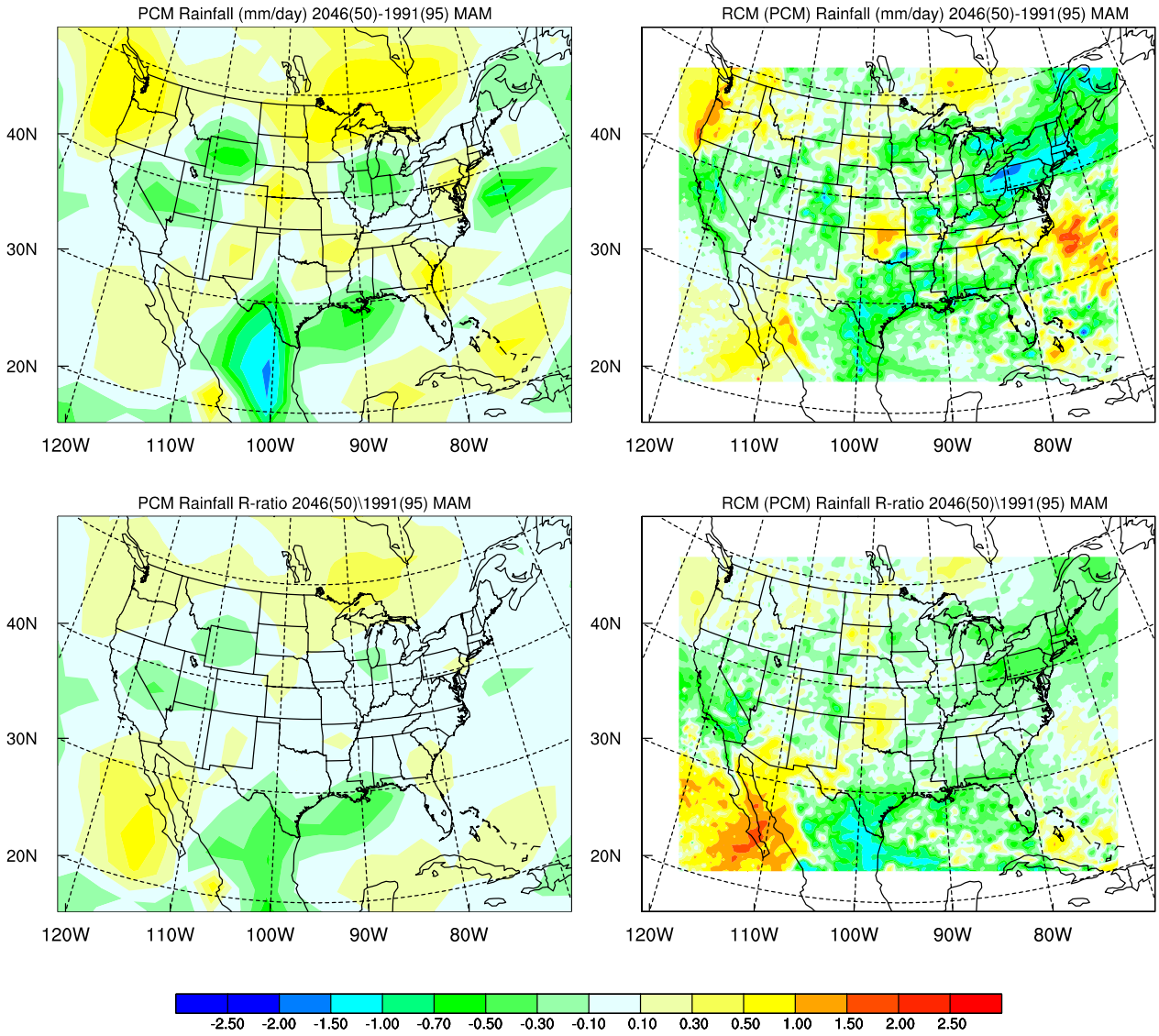

Figure 48. Maps of spring precipitation differences (2046-2050 minus 1991-1995) from (top and bottom left panels) the Parallel Climate Model and (top and bottom right panels) RCM driven by the PCM. Top panels show absolute differences (mm d-1) and bottom panels show these same differences expressed in percent of the PCM value.

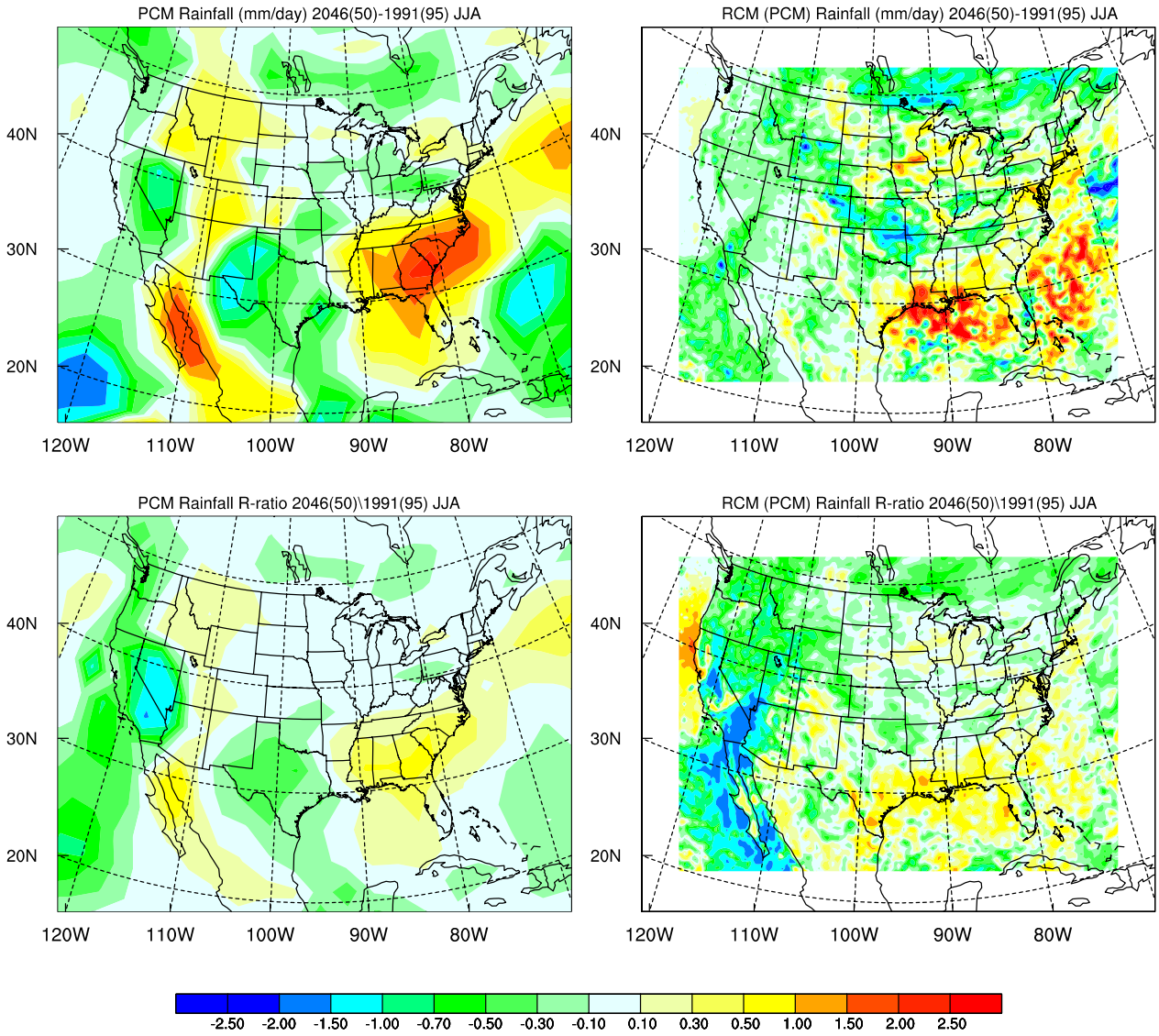

Figure 49. Maps of summer precipitation differences (2046-2050 minus 1991-1995) from (top and bottom left panels) the Parallel Climate Model and (top and bottom right panels) RCM driven by the PCM. Top panels show absolute differences (mm d-1) and bottom panels show these same differences expressed in percent of the PCM value.

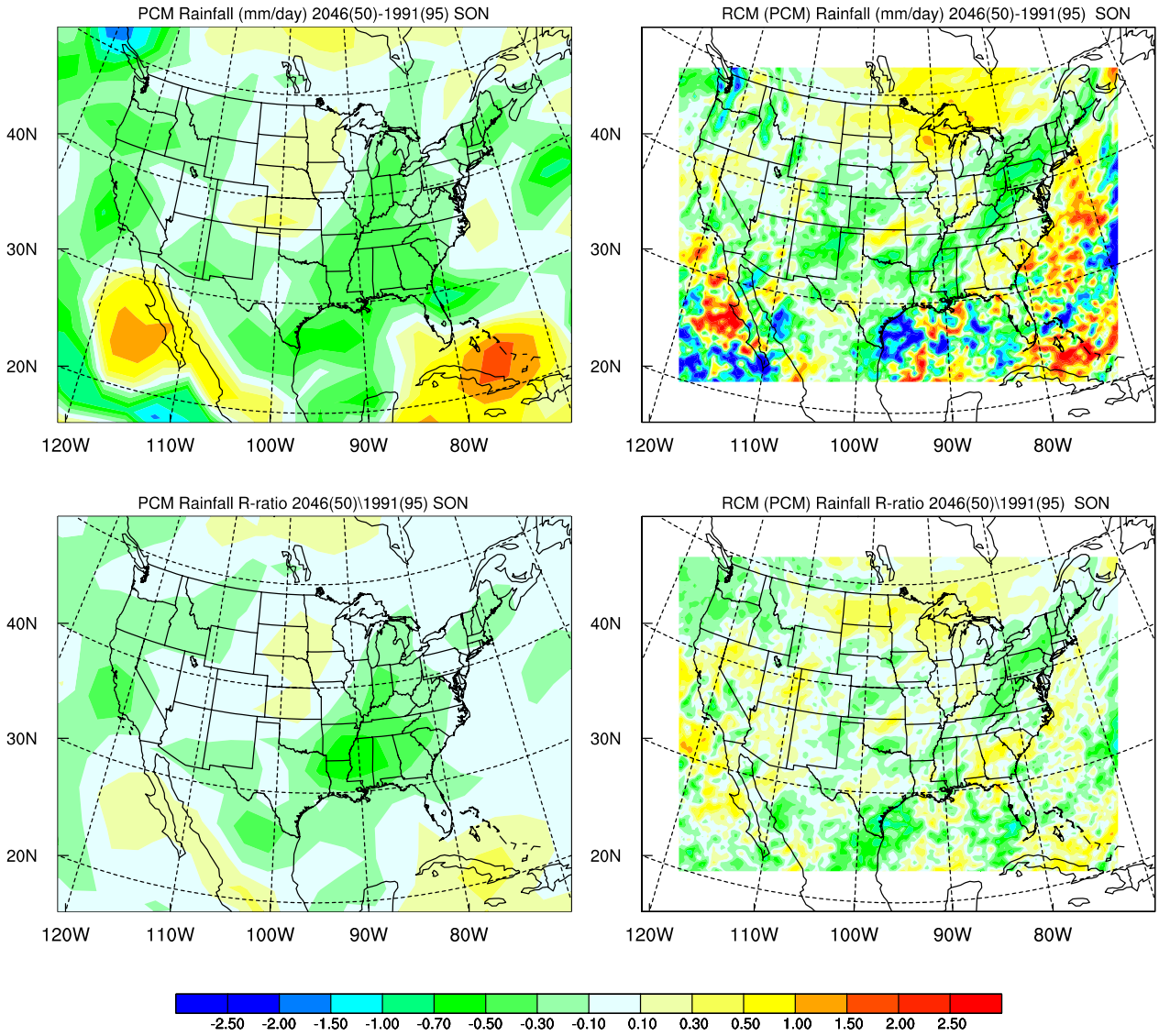

Figure 50. Maps of fall precipitation differences (2046-2050 minus 1991-1995) from (top and bottom left panels) the Parallel Climate Model and (top and bottom right panels) RCM driven by the PCM. Top panels show absolute differences (mm d-1) and bottom panels show these same differences expressed in percent of the PCM value.

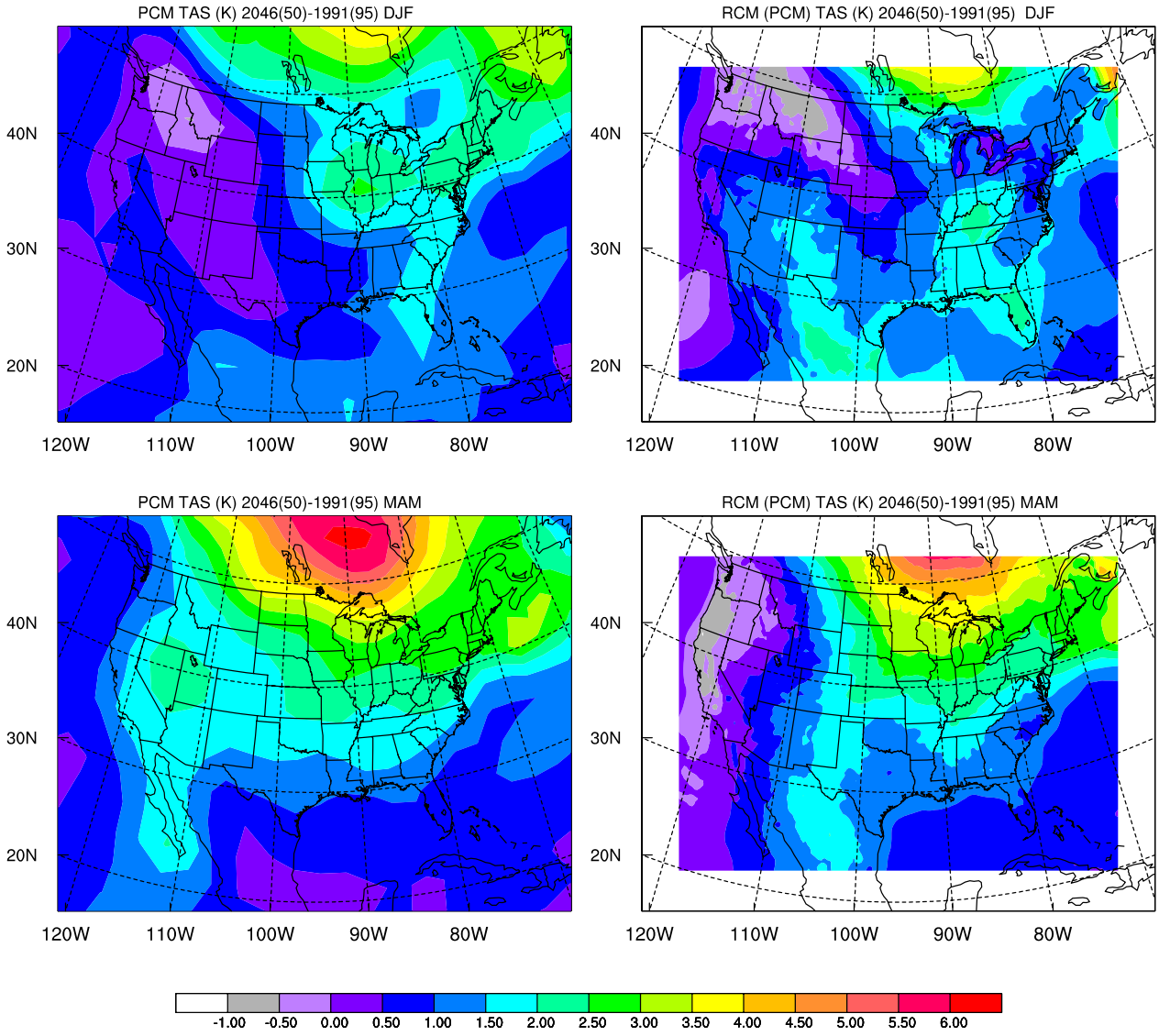

Fig. 51. Maps of temperature differences (2046-2050 minus 1991-1995) from (top and bottom left panels) the Parallel Climate Model and (top and bottom right panels) RCM driven by the PCM. Top panels show winter differences (°C) and bottom panels show spring differences (°C).

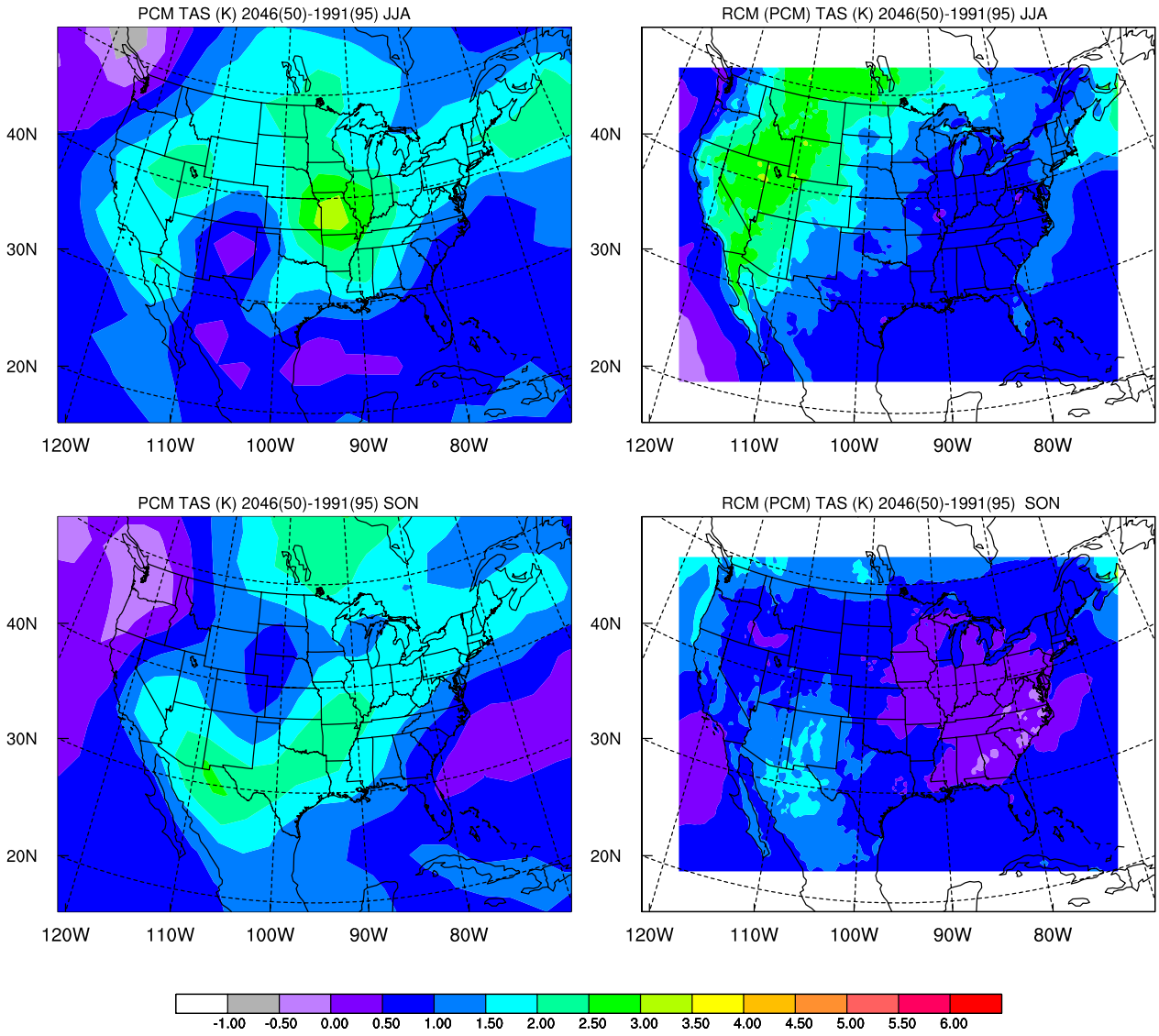

Fig. 52. . Maps of temperature differences (2046-2050 minus 1991-1995) from (top and bottom left panels) the Parallel Climate Model and (top and bottom right panels) RCM driven by the PCM. Top panels show summer differences (°C) and bottom panels show fall differences (°C).

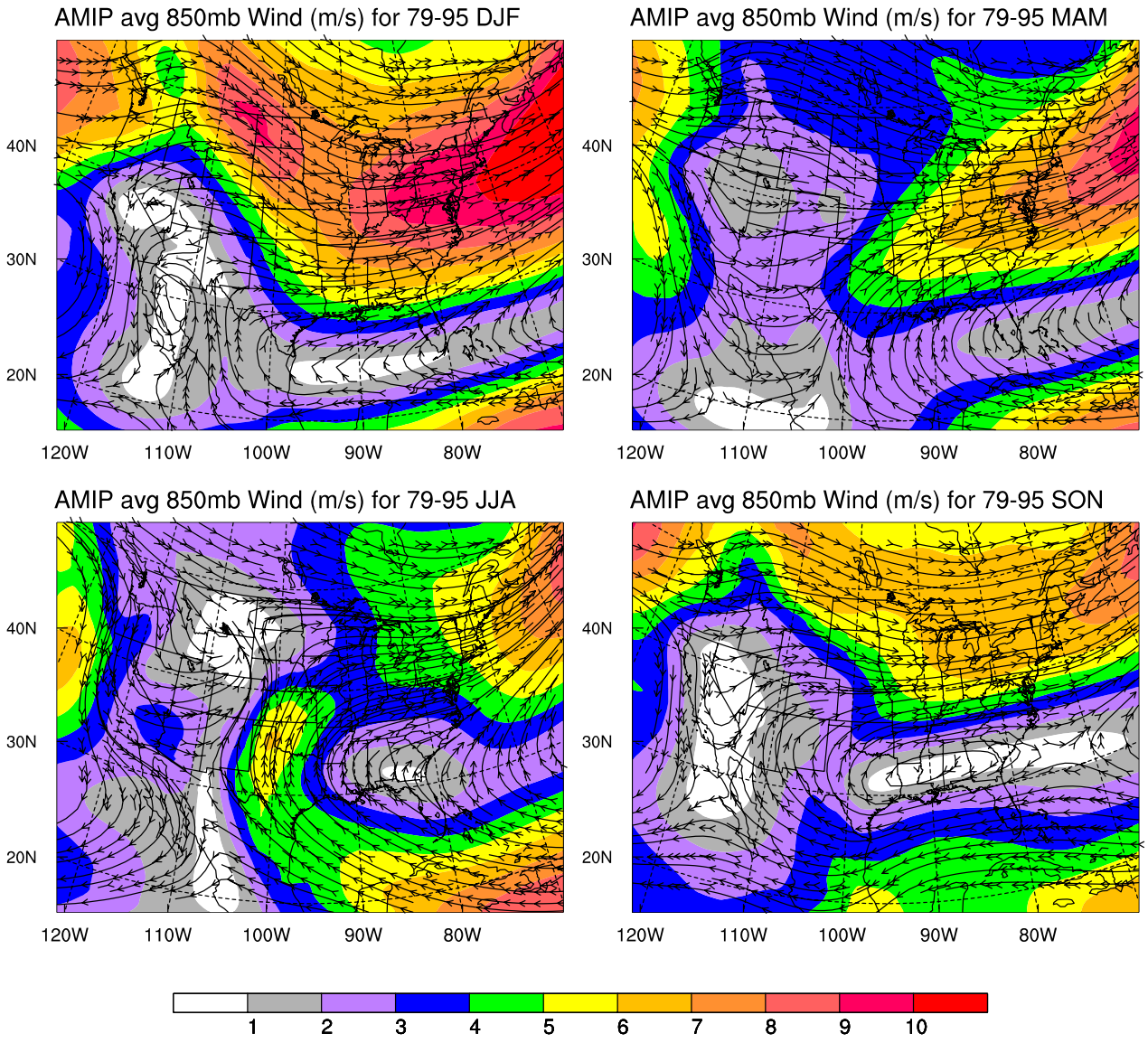

Figure 53. AMIP model composite maps of wind flow at a level of 850 hPa for (top left) winter, (top right) spring, (bottom left) summer, and (bottom right) fall, Barbed lines indicated wind flow directions and colored shading indicates speed (m s^{-1}).

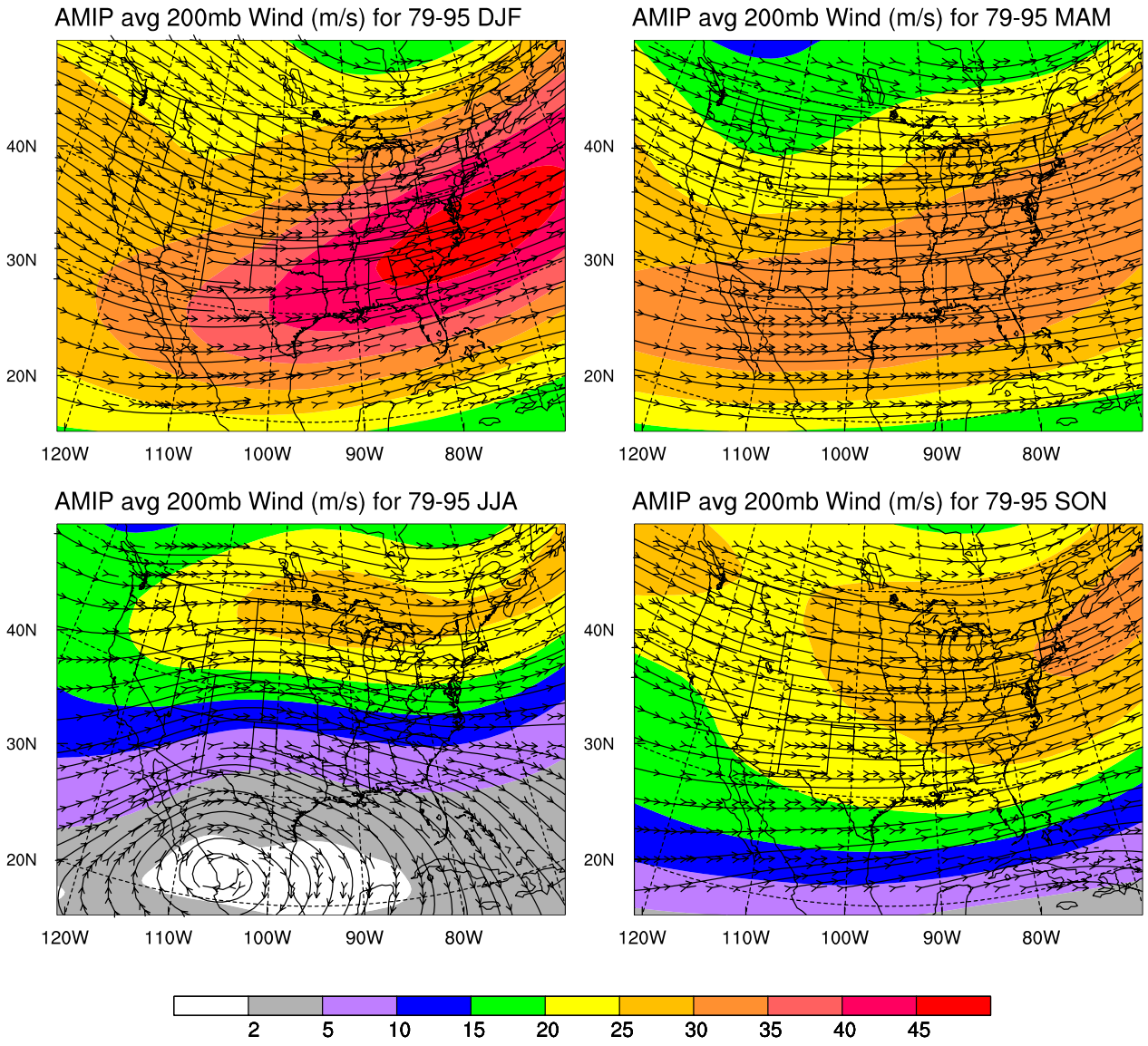

Figure 54. AMIP model composite maps of wind flow at a level of 200 hPa for (top left) winter, (top right) spring, (bottom left) summer, and (bottom right) fall, Barbed lines indicated wind flow directions and colored shading indicates speed (m s^{-1}).

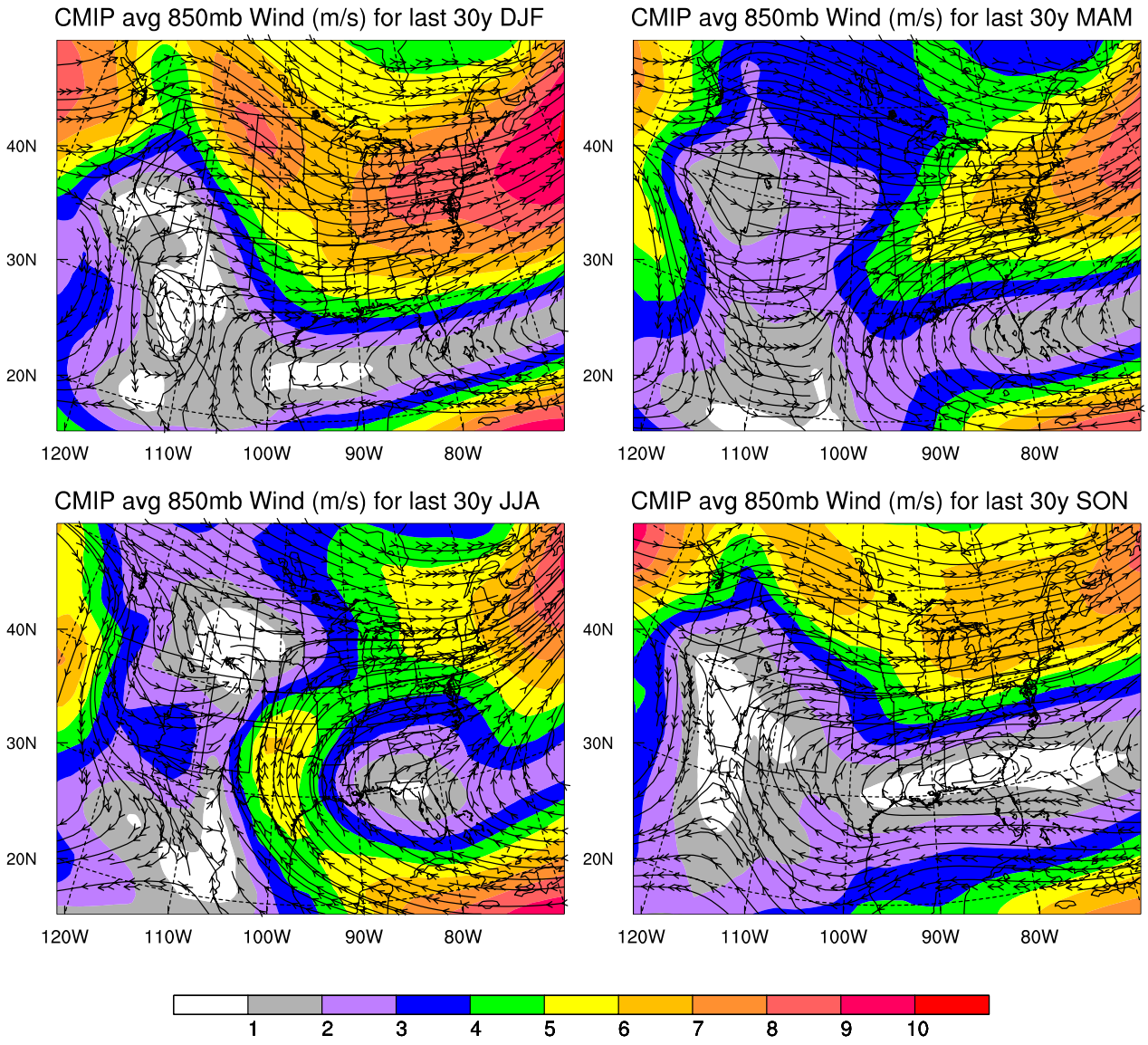

Figure 55. CMIP model composite maps of wind flow at a level of 850 hPa for (top left) winter, (top right) spring, (bottom left) summer, and (bottom right) fall, Barbed lines indicated wind flow directions and colored shading indicates speed (m s^{-1}).

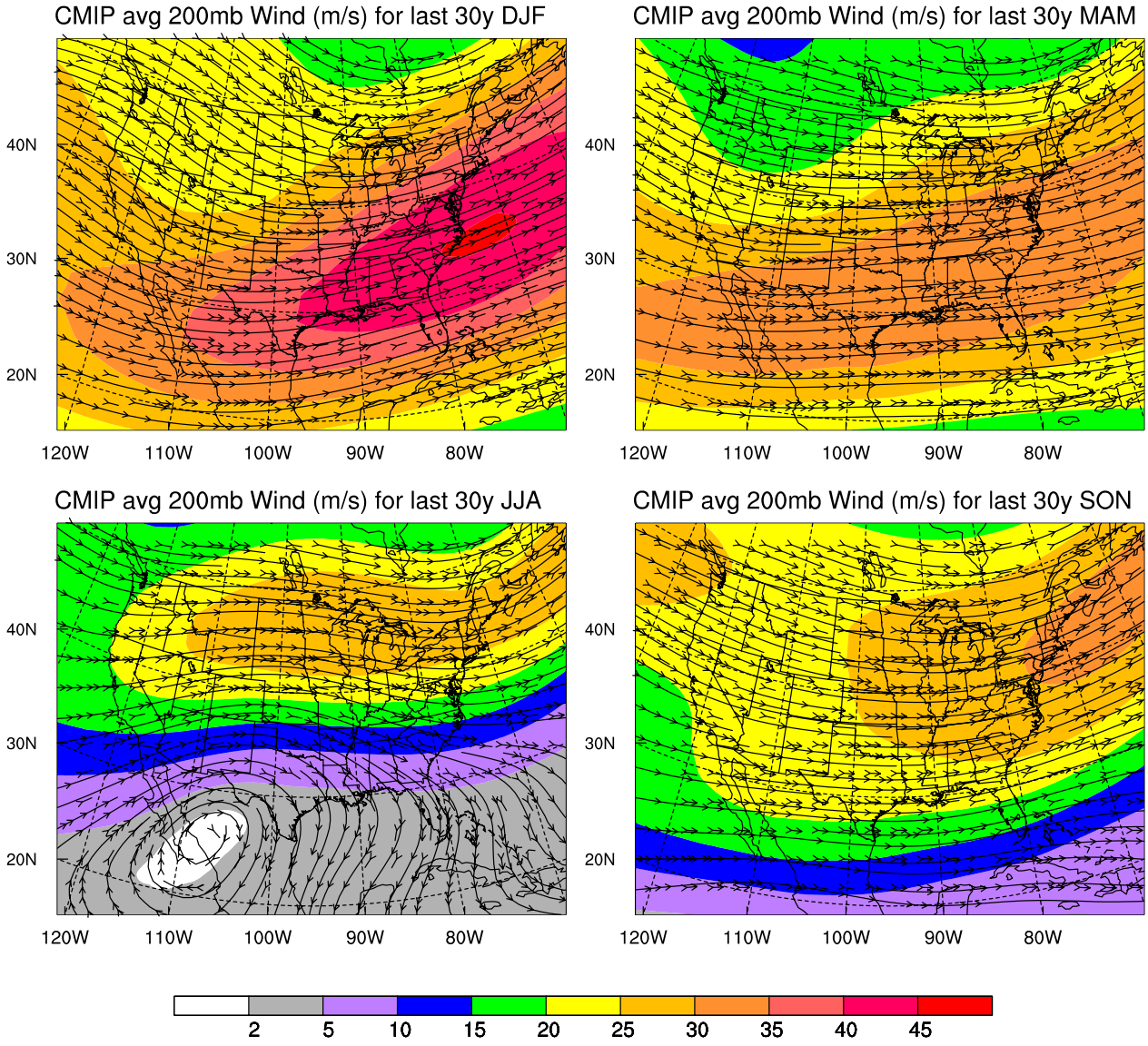

Figure 56. CMIP model composite maps of wind flow at a level of 200 hPa for (top left) winter, (top right) spring, (bottom left) summer, and (bottom right) fall, Barbed lines indicated wind flow directions and colored shading indicates speed (m s^{-1}).

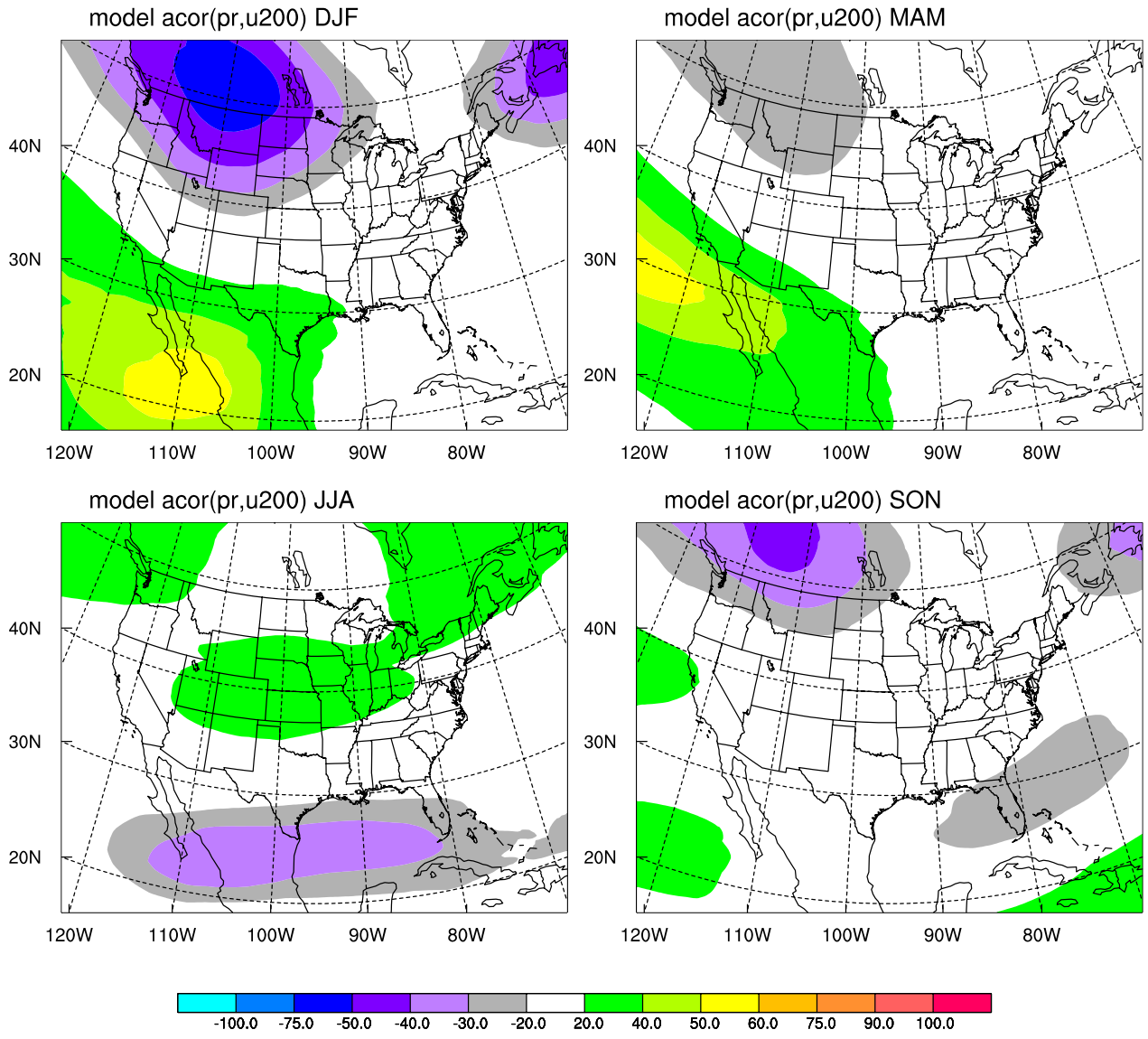

Figure 57. AMIP model composite maps of correlation coefficient between southerly component difference (model-observed) of the wind speed at 850 hPa and precipitation difference (model-observed) in the central U.S. for 4 seasons.

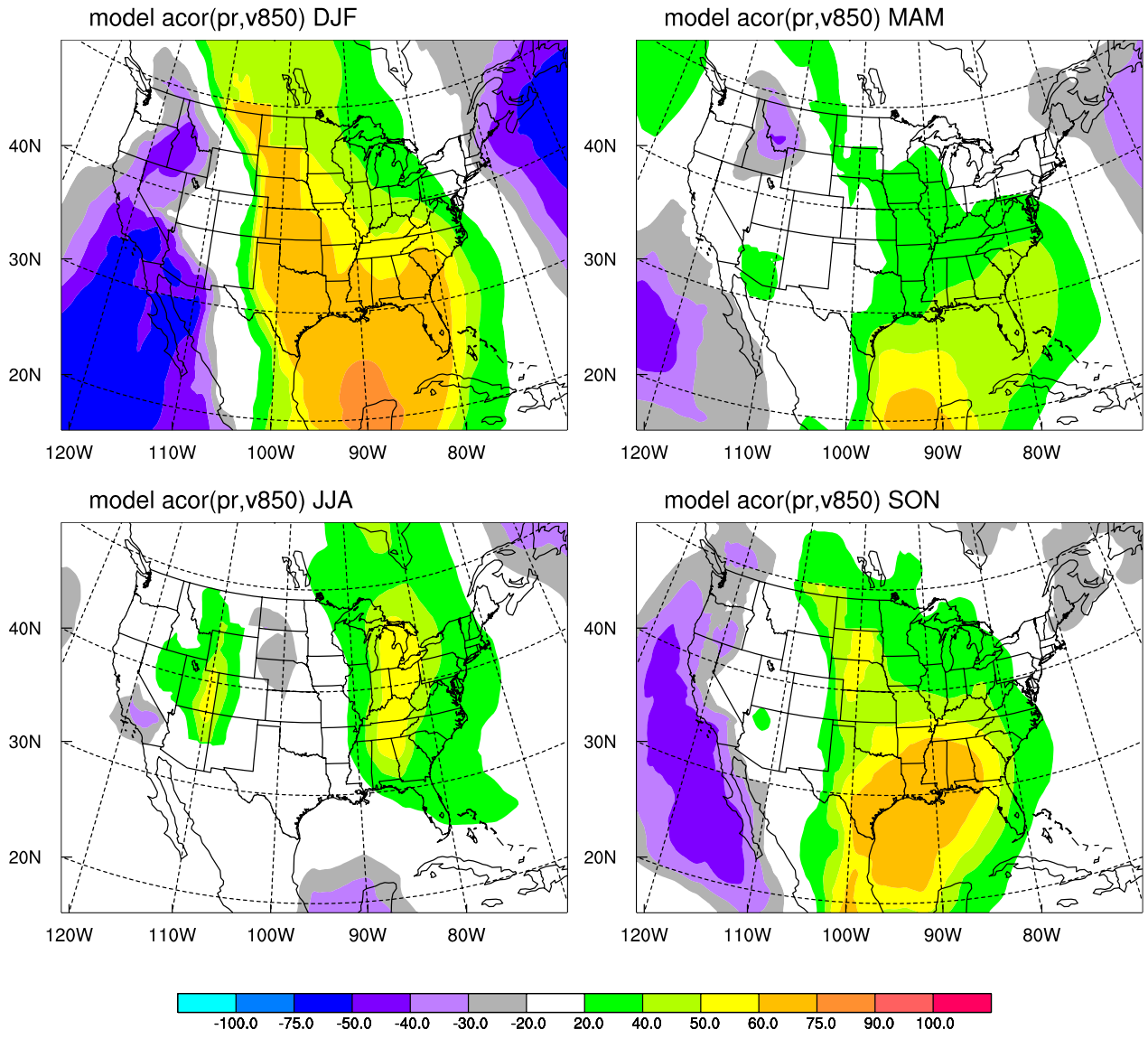

Figure 58. AMIP model composite maps of correlation coefficient between southerly component difference (model-observed) of the wind speed at 200 hPa and precipitation difference (model-observed) in the central U.S. for 4 seasons.